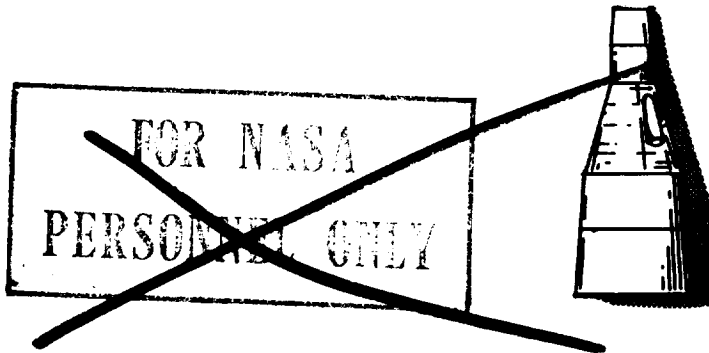


4
Copy No. *8*

NASA Project Gemini Working Paper No. 5003

SIX-DEGREES-OF-FREEDOM GEMINI REENTRY SIMULATION



RECEIVED

SEP 2 1963

RECEIVED
SEP 12 1963

BEST AVAILABLE COPY

DISTRIBUTION AND REFERENCING

(NASA-TM-80371) SIX-DEGREES-OF-FREEDOM
GEMINI REENTRY SIMULATION (NASA) 55 p

N79-77935

Unclas
00/13 28659



NATIONAL AERONAUTICS AND SPACE ADMINISTRATION

MANNED SPACECRAFT CENTER

Houston, Texas

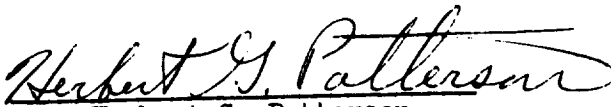
September 12, 1963



NASA PROJECT GEMINI WORKING PAPER NO. 5003

SIX-DEGREES-OF-FREEDOM GEMINI REENTRY SIMULATION

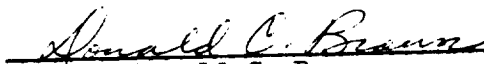
Prepared By:



Herbert G. Patterson
STD, Flight Dynamics Branch

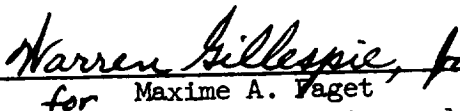


Samuel H. Nassiff
FCOD, Flight Simulation Branch



Donald C. Brown
STD, Flight Dynamics Branch

Authorized for Distribution:


for Maxime A. Yaget

Assistant Director for Engineering and Development

NATIONAL AERONAUTICS AND SPACE ADMINISTRATION

MANNED SPACECRAFT CENTER

HOUSTON, TEXAS

SEPTEMBER 12, 1963

TABLE OF CONTENTS

Section	Page
SUMMARY	1
INTRODUCTION	1
LIST OF SYMBOLS	2
ANALOG SIMULATION	4
Characteristics of Simulated Vehicle	5
Equations of Motion	5
Control System	6
Control Handle	7
Displays	7
TEST PROCEDURE	9
RESULTS AND DISCUSSION	11
Roll Profile	11
Vehicle Motions	12
Fuel Consumption	12
Displays	14
Control Handle	15
Pilot Ratings	16
CONCLUDING REMARKS	16
RECOMMENDATIONS	17
REFERENCES	17
<u>APPENDIX A</u>	
EQUATIONS OF MOTION	18
<u>APPENDIX B</u>	
AERODYNAMIC DATA	22
TABLE I	23
FIGURES 1 to 13(d)	24-52

TABLES

Table		Page
1	JET MOMENTS	25

LIST OF FIGURES

Figure		Page
1	Block diagram of analog simulation	24
2	Axes systems	25
3	Location of control jets	
	(a) General location	26
	(b) Rear view (Xb into paper)	27
4	Block diagram of manual control system	28
5	Hand controller	29
6	Display panel	30
7	Simulator cockpit	31
8	Time histories of commanded roll angles	
	(a) Roll profile A	32
	(b) Roll profile B	33
	(c) Roll profile C	34
9	Time histories of actual roll angles and commanded roll angles	
	(a) Flight 1, roll profile A, rate-command mode . .	35
	(b) Flight 2, roll profile B, rate-command mode . .	36
	(c) Flight 3, roll profile C, rate-command mode . .	37
	(d) Flight 4, roll profile A, direct mode	38
	(e) Flight 5, roll profile B, direct mode	39
	(f) Flight 7, roll profile C, direct mode	40
	(g) Flight 8, roll profile C, direct mode, One ring of control jets	41

LIST OF FIGURES

Figure		Page
10	Time histories of atmospheric entries	
	(a) Flight 3, rate-command mode	43
	(b) Flight 7, direct mode	45
11	Pilot rating sheet	47
12	Pilot rating summary	48
13	Aerodynamic characteristics of simulated vehicle	
	(a) Axial-force coefficient	49
	(b) Normal-force coefficient	50
	(c) Pitching-moment coefficient	51
	(d) Trim conditions	52

SUMMARY

The manually controlled atmospheric entry of the Gemini vehicle was simulated in six-degrees-of-freedom. A fixed-base simulator containing the hand-controller and pilot displays was used to represent the Gemini entry vehicle. An analog computer was used to solve the equations of motion. The manual control system was capable of operating in two modes: rate-command and direct.

Results of this study indicated that both the rate-command mode and the direct mode were acceptable for pilot control during atmospheric entries of the Gemini vehicle. The control tasks could be performed with a somewhat greater degree of accuracy using the control system in the rate-command mode. However, considerably less fuel was utilized with the control system operating in the direct mode.

INTRODUCTION

One of the critical phases of the Gemini mission occurs when the spacecraft enters the earth's atmosphere at speeds near orbital velocity. During this entry phase, the Gemini vehicle has the requirement of maneuvering to a preselected landing site in the presence of decelerations and aerodynamic heating.

Although the Gemini entry vehicle has the general shape of a ballistic body (blunt nose, with rotational symmetry about the longitudinal axis), it has an inherent lifting capability produced by a vertical center-of-gravity displacement with respect to the vehicle's longitudinal axis. This center-of-gravity displacement induces a trim angle of attack which because of the blunt forward surface, produces a lift vector in the opposite direction from the trim angle. To orient the lift vector to any desired roll position, the vehicle can be rolled about the relative velocity vector or stability axis. This orientation, or lift vector modulation, gives the vehicle a maneuvering capability. If the lift vector modulation is done correctly during descent through the earth's atmosphere, the vehicle can be maneuvered to a preselected landing site. The preselected landing site must lie within the downrange and crossrange maneuver capability or "footprint" of the vehicle. The vehicle is equipped with an on-board digital computer which is continuously predicting an impact point based upon the vehicle's present position and velocity. Based on this predicted impact point and the location of the target, the

computer selects a lift vector orientation which will move the predicted impact point toward the target. The lift vector orientation can be controlled automatically or manually by use of the reaction control jets. The lift vector information is displayed to the pilot by means of a roll error indicator located on the display panel. The pilot can nullify the roll error (return the roll error indicator to center position) by rolling the spacecraft about the velocity vector to the commanded roll angle. At the same time the pilot is also required to damp out any oscillatory motions that might be introduced by the cross-coupling torques of the control jets or by initial misalignments and disturbances. These maneuvers are executed by the pilot manipulating the hand controller. The computer continues to command various roll angles until the predicted impact point coincides with the target. At this time, the computer commands a constant roll rate to cancel out the inherent lift of the vehicle. If the predicted impact point should drift off target at any time during the remainder of the flight, the computer commands a lift vector orientation that forces the predicted impact point back on target. When the predicted impact point coincides with the target, the computer once again commands a constant roll rate. This sequence of commands continues until the drogue parachute is deployed at an altitude of approximately 50,000 feet.

A six-degree-of-freedom analog simulation study of Gemini entry was undertaken by the Spacecraft Technology and Flight Crew Operations Divisions. The objective of the study was to evaluate methods and techniques of manual control during the atmospheric entry phase of the Gemini mission.

LIST OF SYMBOLS

a	total applied acceleration, g
$a_{x_r}, a_{y_r}, a_{z_r}$	accelerations along X_r, Y_r, Z_r , "g"
c.g.	center of gravity
C_A	axial-force coefficient
C_M	pitching-moment coefficient
C_N	normal-force coefficient
D	spacecraft reference length, ft.

g	gravitational acceleration, 32.2 ft/sec^2
h	altitude, ft
\dot{h}	time rate of change of altitude, ft/sec
I_x, I_y, I_z	moments of inertia about X_b, Y_b, Z_b , slug-ft ²
L_J, M_J, N_J	control torques about X_b, Y_b, Z_b , ft-lb
M	Mach number
m	mass of spacecraft, slugs
p, q, r	spacecraft angular velocities about X_b, Y_b, Z_b , rad/sec
p_r, q_r, r_r	spacecraft angular velocities about X_r, Y_r, Z_r , rad/sec
$\dot{p}, \dot{q}, \dot{r}$	time rate of change, p, q, r , rad/sec ²
p_c	commanded roll rate, deg/sec
\bar{q}	dynamic pressure, lb/ft ²
R	distance from earth center to spacecraft, ft
R_e	radius of earth, ft
S	spacecraft reference area, ft ²
u, v, w	spacecraft velocities along X_b, Y_b, Z_b , ft/sec
$\dot{u}, \dot{v}, \dot{w}$	time rate of change of u, v, w , ft/sec ²
V_s	velocity of sound, ft/sec
V_t	total velocity, ft/sec
X_a, Y_a, Z_a	aerodynamic forces along X_b, Y_b, Z_b , lb
X_b, Y_b, Z_b	spacecraft body axes

X_e, Y_e, Z_e	earth fixed axes
X_r, Y_r, Z_r	data reference axes
X_{cg}	distance from aerodynamic reference center-of-gravity to spacecraft center-of-gravity, ft
Z_{cg}	center-of-gravity offset from X_b axis along Z_b axis, ft
α	angle-of-attack, deg
α_t	total angle-of-attack, deg
β	angle of sideslip, deg
γ	flight path angle, deg
η	spacecraft resolution angle, deg
ρ	atmospheric density, slugs/ft ³
ψ, θ, ϕ	attitude angles used in the equations of motion, deg
$\dot{\psi}, \dot{\theta}, \dot{\phi}$	time rate of change of ψ, θ, ϕ , deg/sec
ψ_e, θ_e, ϕ_e	flight director attitude angles, deg
ϕ_c	commanded roll angle, deg

ANALOG SIMULATION

The manually controlled Gemini entry simulation was implemented by coupling an analog computer solution of the spacecraft equations of motion to a fixed-base partial simulation of the Gemini cockpit. The cockpit included pilot displays and a three-axes hand controller. The pilot task during the simulated atmospheric entries was to follow pre-programmed roll profiles with the control system operating in either the direct or rate-command mode. A block diagram of the simulation is shown in figure 1.

Characteristics of Simulated Vehicle

The vehicle considered was of the Gemini two-day mission type and had the following physical characteristics:

Mass (m)	130.55	slugs
Roll inertia (I_x)	576.9	slug-ft ²
Pitch inertia (I_y)	1405.0	slug-ft ²
Yaw inertia (I_z)	1405.0	slug-ft ²
Longitudinal c.g. transfer (X_{cg})	0.31	ft
Vertical c.g. location (Z_{cg})	0.142	ft
Reference area (S)	44.2	ft ²
Reference diameter (D)	7.5	ft

Equations of Motion

The equations of motion used for the entry simulation were written in six-degrees-of-freedom which represented summations of forces and moments along and about the three spacecraft body axes (X_b , Y_b , Z_b). A right-handed system of orthogonal coordinate axes was fixed at the spacecraft's center of gravity with the X_b axis parallel to the longitudinal axis of the spacecraft and positive in the direction of the heat shield and the Z_b axis positive in the direction of the vertical center-of-gravity offset. The Y_b axis completed the right-handed coordinate system. A diagram of the spacecraft axes used in the equations and the axes system used for data reduction is shown in figure 2. Another set of orthogonal axes was fixed in the earth with the X_e axis positive toward the east, Y_e positive toward the south, and Z_e positive toward the center of the earth. The spacecraft attitude angles between earth fixed axes and spacecraft axes (order of rotation θ , ψ , ϕ) represented the angular orientation of the spacecraft and, by means of a bias in θ and ψ , also represented the inertial platform gimbal angles. The equations of motion were written for a flat earth model with additional terms added to the force equations to provide curvature in the direction of flight. The velocity of sound and atmospheric density were programed

as functions of altitude, and the aerodynamic coefficients programed as functions of both Mach number and combined wind angle. The equations of motion used for the entry simulation are presented in Appendix A. The aerodynamic coefficients used in the simulation were obtained from reference 1 and are presented in Appendix B.

Control System

Control of the Gemini entry vehicle is accomplished by use of reaction control jets. The location of the two rings of control jets is shown in figures 3(a) and 3(b) and the control jet moments are presented in table I. The control system simulation contained all the jet cross-coupling and jet select logic which describe the physical characteristics of the system. Control jet transport lags or thrust buildup and decay were not simulated because of the short time durations involved. An adjustable hysteresis signal was built into the control system simulation to prevent jet control "chatter" about the control system deadbands. Both the direct and rate-command control modes were programed and could be interchanged for different flights.

Direct mode.- The direct mode of operation was an on-off control system actuated by means of the control handle. When the handle was deflected greater than 50 percent of the total deflection, a relay was closed and the correct jet moments were added to the equations of motion. Deflections less than 50 percent produced no jet moments. Deflections of the hand controller actuated the following control jets which in turn produced vehicle motions about the X_b , Y_b , Z_b axes (neglecting cross-coupling control terms):

handle forward, jets (D + G), +q, small end down
 handle back, jets (C + H), -q, small end up
 handle turned to right, jets (A + F), +r, small end right
 handle turned to left, jets (B + E), -r, small end left
 handle right, jets (A + E), -p, small end rolls right
 handle left, jets (B + F), +p, small end rolls left

Control jet select logic occurred during maneuvers involving both roll and yaw. For example, when the handle was moved to the left and also turned to the right, control jet F was used in both the roll and yaw maneuvers.

Rate-command mode.- Control handle deflections greater than 10 percent produced a linear relationship between the control handle deflections and the commanded roll rate, with a maximum of 20 deg/sec equal to full deflection. Automatic rate damping was provided about the commanded rates with deadbands of ± 1 deg/sec in roll (about X_b) and ± 2 deg/sec in

pitch and yaw (about Y_b and Z_b). Signal mixing was also provided between body roll rate and body yaw rate. When the pilot commanded a roll rate, a yaw rate equal to 20 percent of the roll rate resulted.

Control Handle

The control handle used to actuate the control jets in both the direct and rate-command control modes was a three axes hand controller. The hand controller used in the simulation is shown in figure 5. This hand controller was a prototype model and was the type that will be used in the Gemini spacecraft. Maximum deflection of the hand controller in any direction was 10 degrees. The hand controller was spring loaded so that if no force was applied, the handle would return to the upright position. Movements of the hand controller in the pitch direction (forward and back) were about a pivot point located approximately half way up the handle. Yaw maneuvers were performed by movement of the handle (turned right and left) about the longitudinal axis of the handle. Roll maneuvers were performed by movements of the handle (right and left) about a pivot point at the base of the handle. There was some inherent mechanical "slop" in the pitch direction. Therefore, the pilots had to be careful not to inadvertently actuate the pitch jets while performing yaw and roll maneuvers. This was especially true when the control system was operating in the rate-command mode because of the small stick dead-bands. The physical characteristics of the control handle were as follows:

<u>Maneuver</u>	<u>Break-out Force</u>	<u>Maximum Deflection</u>
Roll	18 to 24 in-lb	18 in-lb
Pitch	18 in-lb	48 in-lb
Yaw	7.5 in-lb	12 in-lb

Displays

The display panel presented to the pilot for the entry simulation consisted of a Gemini all attitude indicator or "eight ball," accelerometer, clock, and a roll rate command light. The display panel is shown in figure 6, and the simulator cockpit is presented in figure 7.

The vertical and horizontal needles on the face of the Gemini eight ball displayed the spacecraft yaw and pitch rates, respectively. Maximum deflection of the needles was 5 deg/sec. Rates about the spacecraft Y_b and Z_b axes produced the following movements of the needles:

- + q, horizontal needle moved up
- q, horizontal needle moved down
- + r, vertical needle moved left
- r, vertical needle moved right

The eight ball itself displayed the gimbal angles of the inertial platform. The platform was aligned prior to retrofire so that a zero reading of the eight ball for pitch, yaw, and roll meant that X_b axis of the spacecraft was aligned with the local horizontal and pointed in the direction of flight. With this alignment, the Y_b and Z_b axes point toward the north and toward the earth, respectively. Therefore, for the spacecraft to be at the proper angular orientation at retrofire, the eight ball would indicate $\psi_e = 180^\circ$, $\theta_e = -16^\circ$, and $\phi_e = 0^\circ$. Positive and negative rotations from the zero orientation of the gyro angles were presented by the following movements of the eight ball:

- + ψ_e , eight ball moved left, small end right
- ψ_e , eight ball moved right, small end left
- θ_e , eight ball moved up, small end down
- + θ_e , eight ball moved down, small end up
- ϕ_e , eight ball rotates right, small end rolls left
- + ϕ_e , eight ball rotates left, small end rolls right

The roll error indicator, which was located above the eight ball, represented a mixed signal of roll position and roll rate error. Maximum deflection of the roll error indicator represented a roll error of 5 deg-deg/sec. However, flights were made with the maximum deflection set at 20 deg-deg/sec to reduce sensitivity. The general expression for the roll error was:

$$\text{error} = (\phi_c - \phi_e) - p \quad (1)$$

$$\text{error} = \pm 20 \text{ deg/sec} - p \quad (2)$$

where ϕ_c is the commanded roll angle of the spacecraft in degrees, ϕ_e the actual roll angle of the spacecraft in degrees, and p the roll rate of the spacecraft in deg/sec. Equation (1) was displayed to the pilot when a roll angle was commanded and equation (2) displayed when a roll rate of 20°/sec was commanded. Positive errors moved the indicator to the left of the center, negative errors moved the indicator to the right of center. Actuation of the roll rate command light indicates a

constant roll rate command. Although the rate command light is not incorporated on the Gemini pilot display panel, it was used in this study to evaluate its possible application in the Gemini spacecraft.

TEST PROCEDURE

The simulated atmospheric entries began subsequent to retrofire at an altitude of approximately 300,000 feet. The initial conditions for all the entries were:

$$u = 23,200 \text{ ft/sec}$$

$$v = 0 \text{ ft/sec}$$

$$w = 7,540 \text{ ft/sec}$$

$$h = 300,000 \text{ ft}$$

$$p = 0 \text{ rad/sec}$$

$$q = 0 \text{ rad/sec}$$

$$r = 0 \text{ rad/sec}$$

$$\gamma = -1.91 \text{ deg}$$

$$\psi = 0 \text{ deg}$$

$$\theta = -19.91 \text{ deg}$$

$$\phi = 180 \text{ deg}$$

$$\psi_e = 180 \text{ deg}$$

$$\theta_e = 108.51 \text{ deg}$$

$$\phi_e = 180 \text{ deg}$$

Typical roll commands of the on-board digital computer were programed on the analog computer. Roll profiles A, B, and C are shown in figures 8(a), 8(b), and 8(c), respectively. Each pilot flew at least seven simulated entries. The first three flights (flights 1, 2, and 3) were performed in the rate-command mode with the pilot attempting to follow roll profiles A, B, and C, respectively. In flights 4 and 5 the pilot

attempted to follow roll profiles A and B with the control system operating in the direct mode. Flight 6 was a constant roll rate in the direct mode, and in flight 7 the pilot attempted to follow roll profile C in the direct mode. Some of the pilots flew an additional flight (flight 8) which was the same as flight 7 but the control jet moments were reduced by a factor of two, representing only a single ring of control jets. The roll error needle indicated error signals generated from equations (1) and (2).

The spacecraft was initially aligned at the correct entry attitude (flight path angle -1.91° , trim angle of attack 18°) with the lift vector pointed away from the earth. The pilot allowed the spacecraft to remain at this orientation until entry into the atmosphere produced aerodynamic moments greater than the cross-coupling torques of the control jets (this condition occurs at approximately 300,000 ft, or at the start of the simulation). At this point, the pilot endeavored to nullify the roll error (return the roll error indicator needle to center position) by rolling the spacecraft about the velocity vector to the commanded roll angle or at the commanded roll rate. At the same time the pilot was also required to damp out any oscillatory motions that might have been introduced by the cross-coupling torques of the control jets or by initial misalignments and disturbances (in the rate-command mode the spacecraft is automatically rate-damped).

In general, the pilot directed the movement of the hand controller in the same direction as the movement of the needles. That is, if the vehicle had a positive angular rate in yaw (+r), the vertical yaw rate needle moved to the left. To correct the yaw rate, the pilot turned the hand controller to the left which fired control jets B and E which produced a negative yaw torque to nullify the spacecraft's angular rate. This corrective action was also true for the roll error indicator as long as the error was being generated by equation (1) (roll angle was being commanded). When the roll error indicator moved to the left of the center position, indicating that the commanded roll angle was greater than the spacecraft's roll angle, the pilot deflected the control handle to the left to produce roll rate which reduced the roll error. When the roll error was being generated by equation (2) (roll rate of 20 deg/sec was being commanded) the roll rate command light came on and the pilot deflected the control handle in the direction of the roll error indicator. When in the direct mode, the pilot returned the control handle to the upright position as soon as a roll rate of 20 deg/sec was achieved (roll error indicator in the center). When in the rate command mode, the pilot kept the control handle at full deflection thereby commanding a roll rate of 20 deg/sec (roll error indicator in the center). The pilot continued to follow this procedure until the roll rate command light went off. At this time the control handle was deflected in the direction of the roll error indicator until the roll angle being commanded was

achieved. This sequence of commands continued until the spacecraft reached an altitude of 50,000 feet, at which time the flights were terminated.

Prior to each set of test flights, the pilots were briefed concerning the analog simulation and about the various aspects involved with a manually controlled Gemini atmospheric entry. The pilots then flew several familiarization flights with the control system operating in both the rate-command and the direct mode to acquaint themselves with the control tasks involved. The test flights are categorized as follows:

<u>Flight</u>	<u>Control Mode</u>	<u>Roll Profile</u>
1	Rate-Command	A
2	Rate-Command	B
3	Rate-Command	C
4	Direct	A
5	Direct	B
6	Direct	Constant roll rate
7	Direct	C
8	Direct (single ring of control jets)	C

RESULTS AND DISCUSSION

Roll Profile

Control ability.- During each of the simulated flights the pilots attempted to follow the preprogrammed roll profile as closely as possible; that is, they attempted to keep the roll error indicator needle centered. Typical time histories of actual roll angles and commanded roll angles for each of the eight flights (except flight 6, which was constant roll rate entry) are shown in figures 9(a) through 9(g). In flights 1 and 4, the pilots flew roll profile A with the control system operating in the rate-command mode and the direct mode respectively. The same control system sequence was used during flights 2 and 5 where the pilots attempted to fly roll profile C. Figures 9(a) and 9(b) show a comparison of the pilot's control ability in the direct and rate-command modes. This comparison shows that the pilots were able to follow the commanded roll profiles with a somewhat greater degree of accuracy in the rate-command mode. The effect of roll control accuracy with respect to range error was not evaluated in this study. One reason for the greater degree

of accuracy was the automatic rate damping system associated with the rate-command mode. Vehicle oscillations were automatically rate damped; thus, the only task the pilots had to perform was to follow the commanded roll angles and command roll rates as closely as possible. Another reason for this better accuracy was that the pilots could command smaller control inputs with the control system in the rate-command mode. Therefore, the pilots were able to hold the vehicle altitude closer to the commanded roll angles.

Vehicle Motions

During each of the simulated flights, time histories of the important vehicle parameters were recorded. Two typical time histories of atmospheric entries are presented in figure 10. Figure 10(a) represents typical time histories of vehicle response and parameters during flight 3 (roll profile C, rate-command mode). Figure 10(b) represents typical time histories of vehicle response and parameters during flight 7 (roll profile C, direct mode). It can be seen that vehicle oscillations were somewhat greater when the pilot was operating the control system in the direct mode. Once again, this was due to the automatic rate damping associated with the rate-command mode. Due to this automatic rate damping, the pilots could forget about vehicle oscillations and concentrate on following the commanded roll angles and commanded roll rates as closely as possible. When the pilots were operating with the control system in the direct mode they not only had to follow the commanded roll angles and commanded roll rates, but they also had to manually damp vehicle oscillations. At first, the pilots had difficulty performing both of the control tasks at the same time. They would first maneuver the vehicle to the commanded angle or rate and then manually rate damp the disturbances. As the pilots became more familiar with the direct mode of manual control, they began to perform both control tasks simultaneously.

Fuel Consumption

General.— The rate-command mode required considerably more fuel than the direct mode for an equivalent entry profile. The main reason for the larger fuel consumption was the automatic rate-damping system associated with the rate-command mode. This automatic rate-damping system automatically actuated the control jets when the vehicle oscillation exceeded the deadband of ± 2 degrees per second in pitch and yaw and ± 1 degree per second in roll about the commanded roll rates. That is, if the pilot commanded a 10 degrees-per-second roll rate with the hand controller and the vehicle exceeded a roll rate of 11 degrees per second or was below 9 degrees per second, the control jets were automatically actuated to restore the vehicle's roll rate to the commanded roll rate. Although the rate-command system with the automatic rate damping constrained

the vehicle to remain within the deadbands, it required a greater amount of fuel than manual rate damping in the direct mode.

Constant roll rate maneuvers.- When the control system was operating in the rate-command mode and the pilot commanded a constant roll rate of 20 degrees per second, a 4-degrees-per-second yaw rate resulted due to signal mixing. If the vehicle was at a high trim angle-of-attack (about 17 degrees) during this constant roll rate, the vehicle would tend to have a yaw rate of approximately 6.1 degrees-per-second ($r = p \tan \alpha_t$). This produced a condition where the vehicle had a tendency to yaw at a rate which exceeded the commanded yaw rate (4 deg/sec) plus the deadband (2 deg/sec) totaling 6 degrees-per-second. The yaw jets, therefore, "slaved" in an attempt to reduce the yaw rate within deadband limits. This condition also occurred at low Mach numbers where the trim angle was small (about 5 degrees).

For a constant roll rate atmospheric entry from an altitude of 300,000 feet down to 50,000 feet, the fuel consumed with the control system in the rate-command mode was 17.1 pounds compared to 3.2 pounds with the control system operating in the direct mode (assumptions: specific impulse = 287 pounds-second/pound, thrust per jet = 25 pounds). The difference was not quite as pronounced when typical entry maneuvers were performed. For example, the average values of the fuel consumed during flights 3 and 7 were 22.7 pounds and 13.1 pounds, respectively. Another reason for the greater amount of fuel usage when the control system operated in the rate-command mode was the greater sensitivity of the rate-command mode. Because of this greater sensitivity, the pilots were able to contain the perturbations about the commanded roll angles with a greater degree of accuracy. However, the closer the pilots were able to follow the roll profiles, the more control maneuvers were required and, therefore, the more fuel expended.

Roll attitude maneuvers.- When the vehicle was in a constant roll rate and the roll error indicator commanded a roll attitude, the commanded roll direction was always a function of position error. Regardless of the magnitude and direction of the roll rate, the commanded direction of roll attitude from the onboard computer was always in the direction of the smallest angular rotation. Therefore, there were conditions where the pilots stopped the roll rate in one direction and established a new roll rate in the opposite direction to attain commanded roll angles. However, with the vehicle's relatively high control acceleration of approximately $.21 \text{ rad/sec}^2$, the time required to reverse the roll rate was small and thus the resulting inefficiency also small.

Single ring of control jets.- During flight 8, the control jet moments (presented in table I) were reduced by a factor of two to simulate a single ring of control jets. The pilots found that it was somewhat

easier to manually damp vehicle oscillations when flying with only one ring of control jets. This was probably due to the reduction of cross-coupling control moments and the subsequent reduction in vehicle disturbances. A reduction in fuel consumption also occurred. For example, typical fuel usage for flight 7 was 13.1 pounds. When the same flight was flown with the single ring of control jets (flight 8), the fuel usage was only 9.37 pounds. However, because of the reduction in control moments, more time was required to start and stop roll rates. Therefore, the pilots were not able to follow the commanded roll rates and roll angles as well as with the double ring of control jets.

Displays

Roll error indicator.- The maximum deflection of the roll error indicator was first set with the maximum deflection equal to 5 deg-deg/sec which made the indicator extremely sensitive and difficult to fly. When the vehicle was in a constant roll rate and a roll position was commanded, the pilots would invariably overshoot the commanded roll angle. When the maximum deflection was increased to 20 deg-deg/sec the pilots were able to anticipate movements of the hand controller and hence were able to stop the vehicle at or near the commanded roll angles.

Accelerometer.- The accelerometer was useful for the pilots to determine "g" profiles and as an indication of increasing and decreasing dynamic pressure. At the beginning of the simulated flights (altitude = 300,000 feet), the dynamic pressure was low and therefore the static aerodynamic moments were also low. Due to these low aerodynamic restoring moments, control inputs had a tendency to disturb the vehicle from its initial trim condition. Thus, if the accelerometer indicated a low dynamic pressure, the pilots avoided large control maneuvers. Once the accelerometer indicated an increase in dynamic pressure, the pilots damped the vehicle oscillations and proceeded with the commanded control tasks.

All attitude indicator.- The eight ball displayed angular motions of the vehicle to the pilots. When the pilots flew with the control system in the direct mode and a roll rate reversal was commanded, the eight ball was the pilot's only indication of vehicle roll rate. The black strip on the eight ball was used in determining lift vector orientation.

Roll rate command light.- The roll rate command light appeared to help the pilots determine when a roll rate rather than roll attitude was being commanded. However, when the light was not used, the pilots had no difficulty in following the various roll profiles. After suitable pilot orientation, the roll rate command light appeared to serve no useful purpose.

Rate indicators.- The pitch and yaw rate indicators located on the face of the Gemini eight ball seemed to be extremely sensitive to vehicle

motions. When the vehicle rates exceeded 5 deg/sec, the rate indicator pegged and it became impossible for the pilots to determine the actual yaw rate of the vehicle. Even when the vehicle oscillations were kept to a minimum, the yaw rate indicator still pegged due to the combination of body yaw rate and body roll rate required to produce a roll rate about the stability axes. For example, when a 20 deg/sec roll rate was commanded about the body roll axis and the trim angle of attack was 17 deg, there was a tendency for the vehicle to yaw at a rate of 6.1 deg/sec and the yaw rate indicator always read full scale. If the pilot was operating the control system in the direct mode during this maneuver, it was very difficult to manually damp the vehicle in yaw.

Because of the pegged condition of the yaw rate indicator, the sensitivity of the rate indicators was reduced for some flights so that 10 deg/sec was equal to full deflection. The pilots who flew the simulation with this reduced sensitivity of the rate needles indicated that the pegging of the yaw rate indicator was alleviated and the movements of the needles were greatly improved.

Another method that might be used to alleviate the pegged condition of the yaw rate indicator during roll rate maneuvers is to display the vehicle rates about the stability axis. The stability axis changes with trim angle-of-attack and thus an average value of trim angle-of-attack should be selected for the stability axis. This would greatly reduce the yaw bias associated with roll maneuvers and prevent pegging of the yaw rate indicator. Although this method of displaying spacecraft rates during entry seemed promising, time did not allow for its evaluation during this study.

Control Handle

Once the pilots familiarized themselves with the sensitivity and jet responses of the control handle operation in the rate-command mode, there was little or no trouble in accomplishing the commanded control tasks. However, when the control handle was operating in the direct mode, the pilots required some additional practice and special pilot techniques to accomplish the same control tasks. The pilots found the most efficient way to perform maneuvers with the control system operating in the direct mode was to use short, sharp inputs to the control handle. Because of the type of inputs required, the 50-percent travel or 5-degree deflection of the hand controller required to actuate the control jets in the direct mode was judged by the pilots to be too large. This conclusion was based upon flights in a "shirt-sleeve" environment. However, when the pilots fly the actual vehicle under true environmental conditions, the 50-percent deflection associated with the direct mode may be necessary.

Pilot Ratings

During each of the production flights, the pilots were given a pilot rating sheet (fig. 11). After each flight, the pilots rated the various components of the simulation as indicated below:

- (1) Eight ball indicator
- (2) Pitch and yaw indicators
- (3) Roll error indicator
- (4) Hand controller
- (5) Control jet moments and vehicle response
- (6) Integrated system

The results of the pilot ratings are shown in figure 12. All the mean value ratings fell between rating code 2 (good) and 4 (acceptable). Each component seemed to be rated about the same regardless of the manual mode of operation except for the yaw and pitch indicators. This was due to the pegged condition encountered during constant roll rate maneuvers. The vehicle was automatically rate-damped in the rate command mode and the position of the yaw needle was of little importance. When the vehicle was controlled with the direct mode, manual rate-damping was required and the pegged condition of the yaw indicator needle became quite bothersome.

CONCLUDING REMARKS

Results of the analog simulation study may be summarized as follows:

1. Both the rate-command mode and the direct mode of manual control were found to be acceptable for pilot control.
2. The pilots were able to perform the required control tasks with a somewhat greater degree of accuracy using the control system in the rate-command mode; however, considerably less fuel was utilized with the pilots operating the control system in the direct mode. From an operational standpoint sufficient accuracy should be possible in the direct mode.
3. When the control system was reduced to a single ring of control jets, there was a considerable conservation of fuel and the pilots found that it was somewhat easier to manually damp vehicle oscillations; however, it required more time to start and stop required roll rates. Therefore, the pilots were not able to follow the commanded roll rates and roll angles as well as with the double ring of control jets.

4. The roll error indicator appeared adequate as long as the maximum needle deflection was set at 20 deg-deg/sec.

5. The accelerometer was useful for the pilot to determine "g" profiles and as an indication of increasing and decreasing dynamic pressure.

6. A 5 deg/sec maximum deflection of the rate indicator needles appeared to be too sensitive. During 20 deg/sec constant roll rate maneuvers, the yaw needle sometimes became pegged thereby making it difficult for the pilots to manually damp vehicle yaw oscillations. Displaying vehicle rates about the stability axes would alleviate this pegged condition.

7. The 50-percent travel of the hand controller required to actuate the control jets in the direct mode was judged by the pilots to be too large for this static simulation but may be necessary under actual environmental conditions.

RECOMMENDATIONS

1. For entry, the maximum indication of the rate indicator needles be increased from 5 deg/sec to 10 deg/sec.

2. For entry, the maximum indication of the roll error needle be increased from 5 to 20 deg-deg/sec.

3. Consideration be given to displaying vehicle rates about the stability axes during entry.

REFERENCES

1. Aerodynamic Information Note 20, Gemini Mission Aerodynamics, December 27, 1962.

APPENDIX A

EQUATIONS OF MOTION

The programing of the complete equations of motion for an arbitrarily shaped body with six-degrees-of-freedom presents a formidable task, even if a computer of unlimited size is available. A careful analysis of the physical problem involved in the desired simulation usually reveals that a number of simplifications can be made, with negligible errors resulting. The equations described herein are applicable to entry vehicles of the Gemini type and incorporate the following assumptions:

- (1) The vehicle has external rotational symmetry about its longitudinal axis.
- (2) The vehicle has symmetrical mass distribution about its longitudinal axis (products of inertia are small).
- (3) The earth's gravitational field is constant.
- (4) The earth model is assumed to be flat (additional terms (V_t^2/R) are added to the force equations to provide curvature in the direction of flight.
- (5) Atmospheric density is a function of altitude only.

The derivation of the equations of motion is straight-forward, and may be found in several texts on elementary mechanics. Therefore, the equations are presented here without derivation.

Force Equations

$$\begin{aligned}\dot{u} &= rv - qw + \frac{X_a}{m} + (-\cos \psi \sin \theta) \left(g - \frac{V_t^2}{R} \right) \\ \dot{v} &= pw - ru + \frac{Y_a}{m} + (\sin \psi \sin \theta \cos \phi + \cos \theta \sin \phi) \left(g - \frac{V_t^2}{R} \right) \\ \dot{w} &= qu - pv + \frac{Z_a}{m} + (\cos \theta \cos \phi - \sin \psi \sin \theta \sin \phi) \left(g - \frac{V_t^2}{R} \right)\end{aligned}$$

Moment Equations

$$\dot{p} = \left(\frac{I_x - I_z}{I_x} \right) qr - \left(\frac{Z_{cg}}{D} C_N \sin \eta \right) \frac{\bar{q} SD}{I_x} + \frac{L_J}{I_x}$$

$$\begin{aligned} \dot{q} = & \left(\frac{I_z - I_x}{I_x} \right) pr + \left(C_M \cos \eta - \frac{X_{cg}}{D} C_N \cos \eta \right. \\ & \left. + \frac{Z_{cg}}{D} C_A + \frac{C_{mq} qD}{2 V_t} \right) \frac{\bar{q} SD}{I_x} + \frac{M_J}{I_x} \end{aligned}$$

$$\begin{aligned} \dot{r} = & \left(\frac{I_x - I_y}{I_z} \right) pq + \left(-C_M \sin \eta + \frac{X_{cg}}{D} C_N \sin \eta \right. \\ & \left. + \frac{C_{mq} rD}{2 V_t} \right) \frac{\bar{q} SD}{I_z} + \frac{N_J}{I_z} \end{aligned}$$

Gyro Angles, Euler Angles θ, ψ, ϕ

$$\dot{\psi} = q \sin \phi + r \cos \phi$$

$$\dot{\theta} = \frac{q \cos \phi - r \sin \phi}{\cos \psi}$$

$$\dot{\phi} = p - \dot{\theta} \sin \psi$$

Aerodynamic Forces

$$X_a = -C_A \bar{q} S$$

$$Y_a = -C_N \bar{q} S \sin \eta$$

$$Z_a = -C_N \bar{q} S \cos \eta$$

Auxiliary Equations

$$V_t = (u^2 + v^2 + w^2)^{\frac{1}{2}}$$

$$\sin \eta = \frac{v}{(v^2 + w^2)^{\frac{1}{2}}}$$

$$\cos \eta = \frac{w}{(v^2 + w^2)^{\frac{1}{2}}}$$

$$\sin \alpha_t = \frac{(v^2 + w^2)^{\frac{1}{2}}}{V_t}$$

$$R = R_e + h$$

$$\begin{aligned} \dot{h} = & u(\cos \psi \sin \theta) + v(-\sin \psi \sin \theta \cos \phi - \cos \theta \sin \phi) \\ & + w(\sin \psi \sin \theta \sin \phi - \cos \theta \cos \phi) \end{aligned}$$

$$\bar{q} = \frac{1}{2} \rho V_t^2$$

$$a = \frac{1}{mg} (X_a^2 + Y_a^2 + Z_a^2)^{\frac{1}{2}}$$

$$M = \frac{V_t}{V_s}$$

$$\alpha = \tan^{-1} \frac{w}{u}$$

$$\beta = \sin^{-1} \frac{v}{V_t}$$

Functions of h

$$\rho, V_s$$

Inputs

$$\psi, \theta, \phi, u, v, w$$

$$h, p, q, r$$

Constants

$$m, I_x, I_y, I_z, X_{cg}, Z_{cg}$$

$$S, D, g, C_{mq}, R_e$$

Functions of $\sin \alpha_t$ and M

$$C_A, C_N, C_M$$

APPENDIX B

AERODYNAMIC DATA

The aerodynamic characteristics of the simulated vehicle are presented in figures 13(a) through 13(d). The wind tunnel data points are represented by circular symbols and the aerodynamic coefficients used in the simulation are represented by solid lines. The aerodynamic coefficients were programed on the analog computer as functions of both Mach number and total angle of attack in the following manner:

(1) The aerodynamic coefficients were expressed as functions of both the logarithmic values of Mach number and sine of total angle of attack for ease of analog operation, and

(2) The aerodynamic coefficients were then written as polynomial expressions for various Mach numbers and angle of attack. The coefficients of the polynomial were programed on diode-function-generators. It is estimated that the total error including the polynomial approximations was in the order of 5 to 10 percent. The dynamic aerodynamic coefficient (C_{mq}) used in the equations of motion was programed as a constant and was set to zero for most of the flights. The pitching-moment coefficients presented in figure 13(c) were taken about the aerodynamic reference center of gravity (vehicle station 140.34 in.). The intersection of the spherical and conical sections of the Gemini entry vehicle is reference station 103.44 in. Therefore, to transfer the pitching moment coefficients to the vehicle center of gravity (Station 136.62) the term X_{cg} used in the equations of motion becomes ($X_{cg} = .31$ ft.).

TABLE I.- JET MOMENTS

Jet Moment Components (Ft-Lb)

Jet	Moment about X_b	Moment about Y_b	Moment about Z_b
A	-68.74	21.79	189.25
B	68.74	21.79	-189.25
C	62.94	-189.25	-21.79
D	-61.99	189.25	-21.79
E	-55.66	-21.79	-189.25
F	55.66	-21.79	189.25
G	61.99	189.25	21.79
H	-62.94	-189.25	21.79

Jet Moment Combinations (Ft-Lb)

Desired maneuver	Jets	Moment about X_b	Moment about Y_b	Moment about Z_b
+ Roll	B + F	124.4	0	0
- Roll	A + E	-124.4	0	0
+ Pitch	D + G	0	378.5	0
- Pitch	C + H	0	-378.5	0
+ Yaw	A + F	-13.08	0	378.5
- Yaw	B + E	13.08	0	-378.5
+ Roll + Yaw	B + F + A	55.66	21.79	189.25
+ Roll - Yaw	B + F + E	68.74	-21.79	-189.25
- Roll + Yaw	A + E + F	-68.74	-21.79	189.25
- Roll - Yaw	A + E + B	-55.66	21.79	-189.25

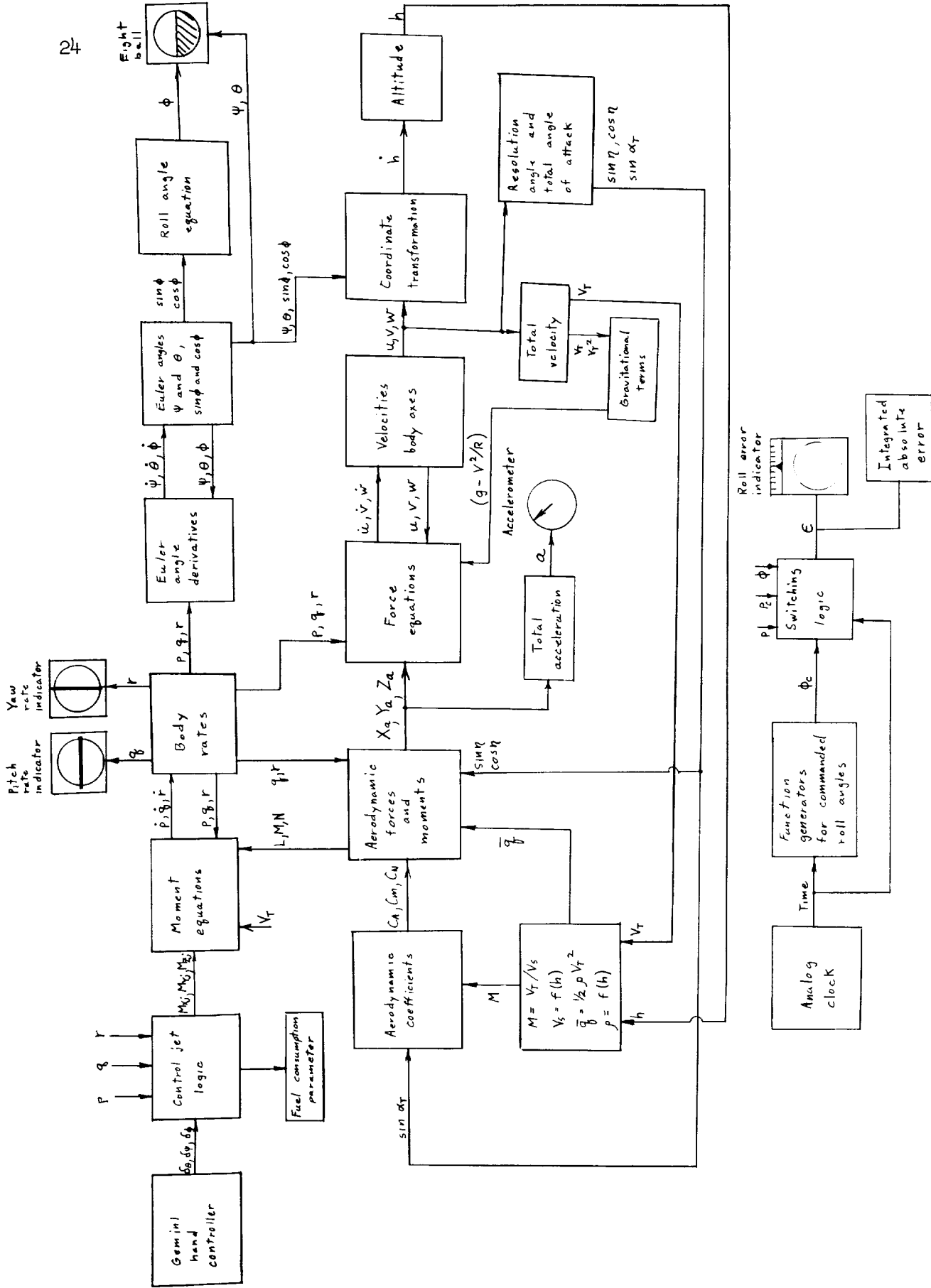


Figure 1.- Block diagram of analog simulation.

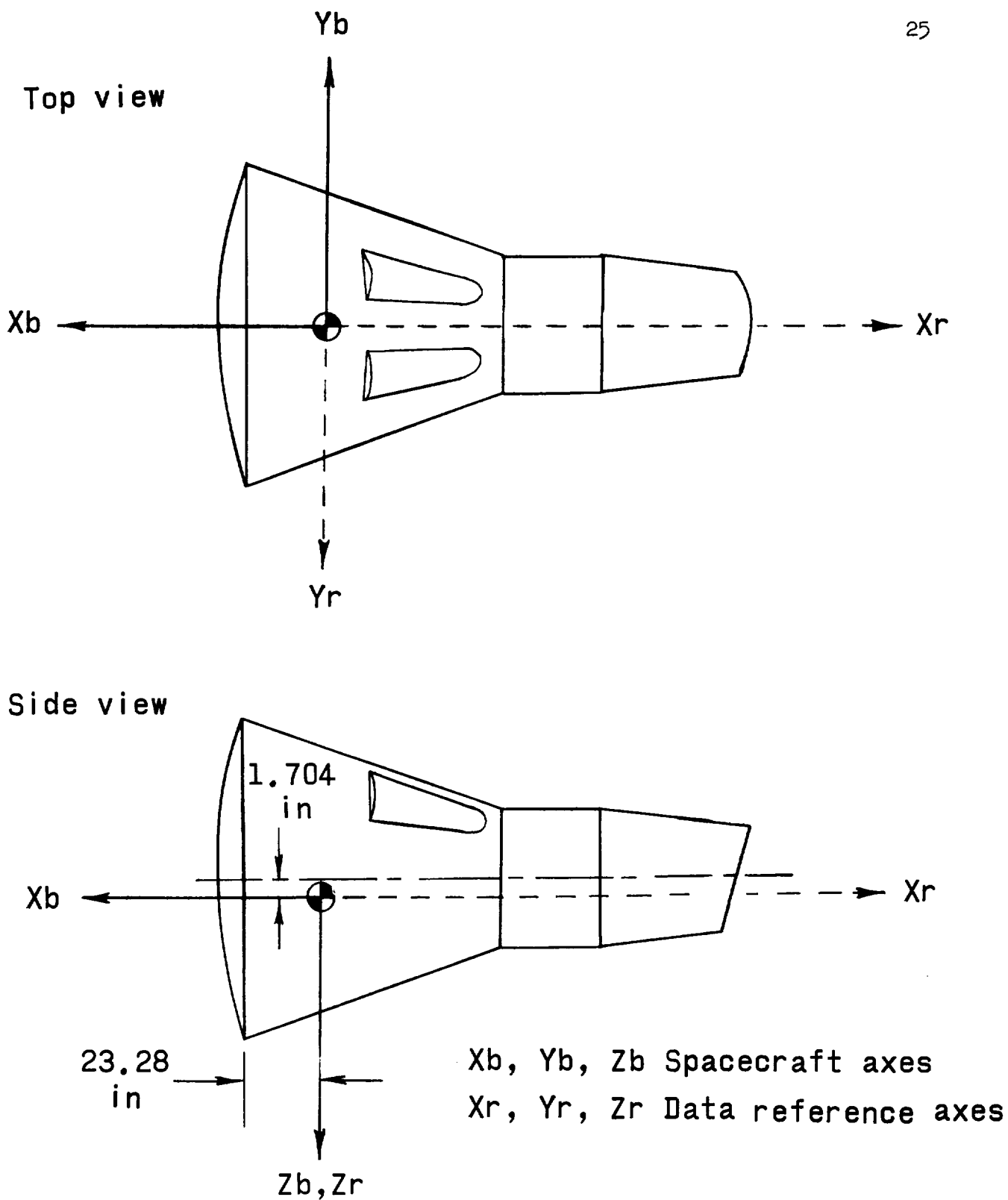
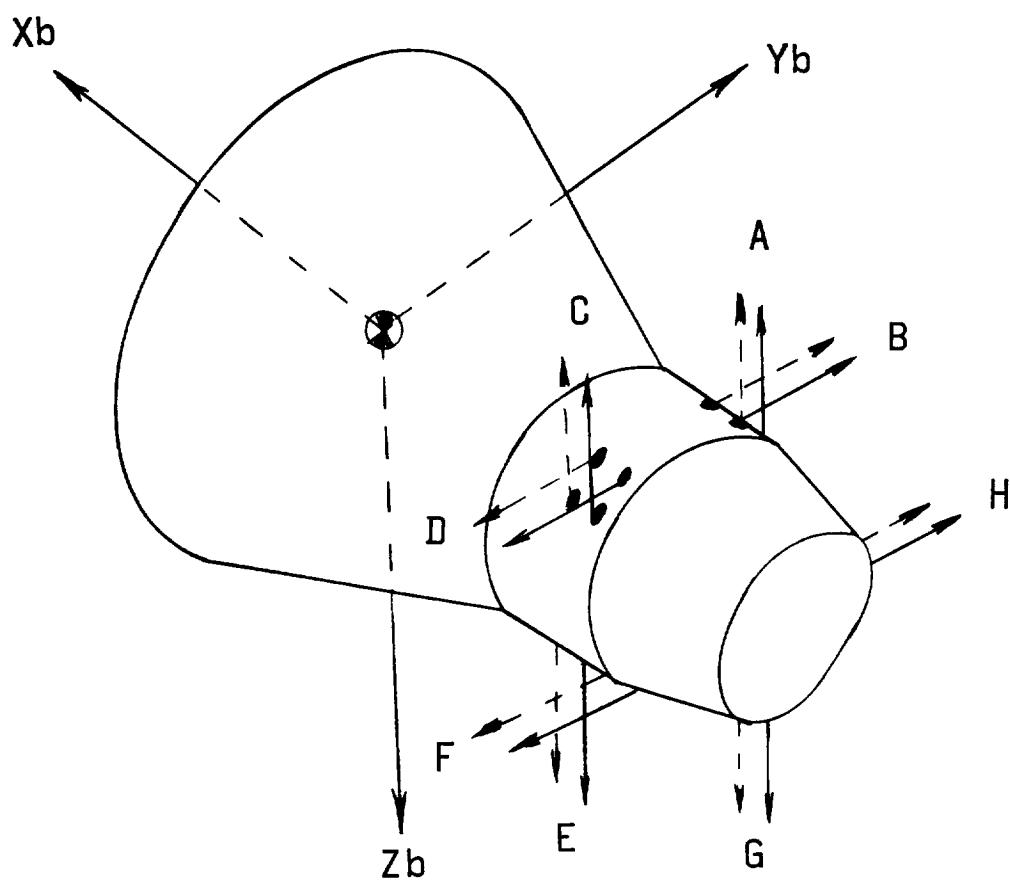


Figure 2.- Axes systems.

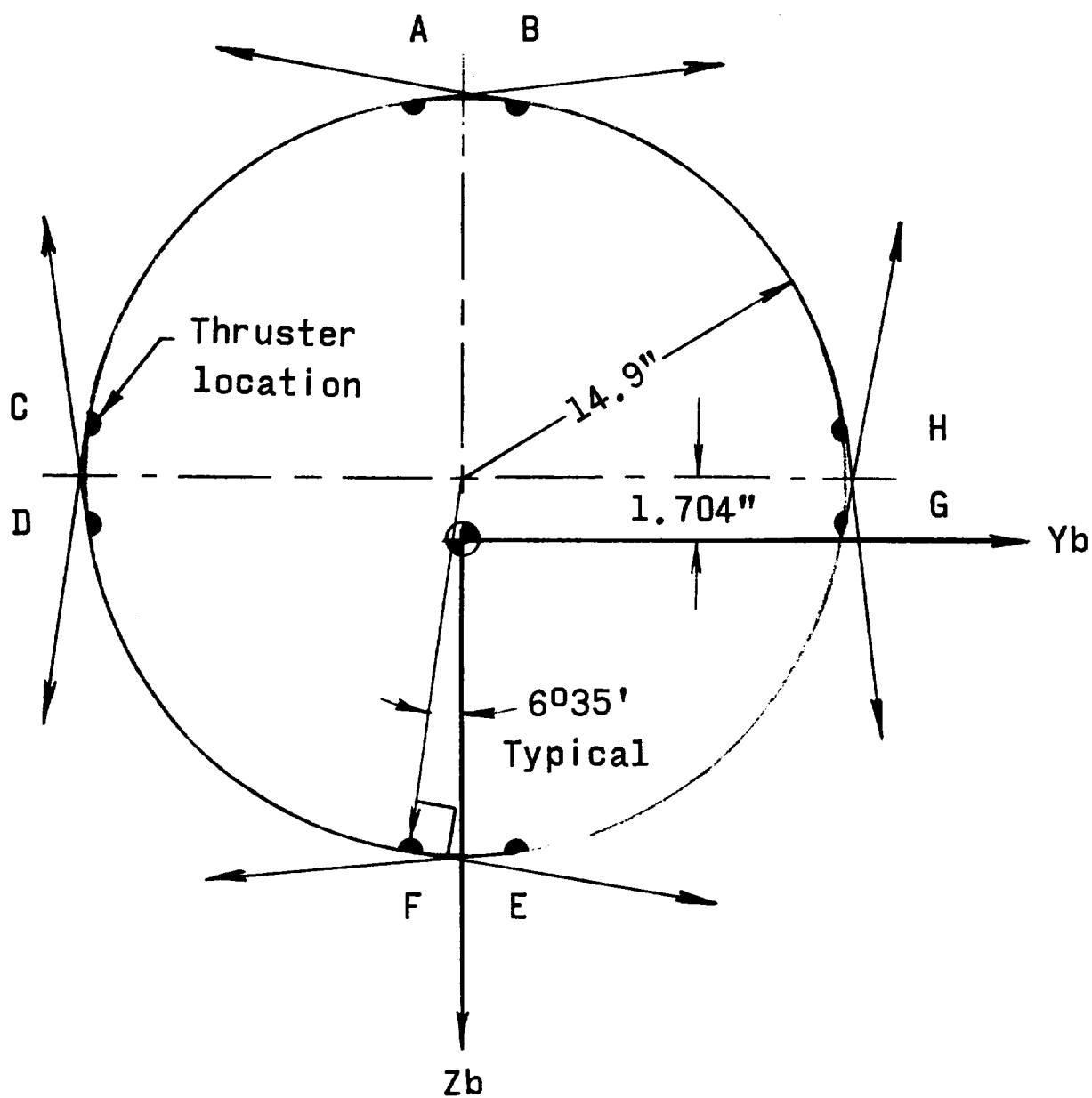
Quantity	Vehicle station
Center of gravity	136.62 in
———— Ring I	188.77 in
----- Ring II	183.77 in



Note: Arrows indicate flow of exhaust gases for 25 lb/thruster.

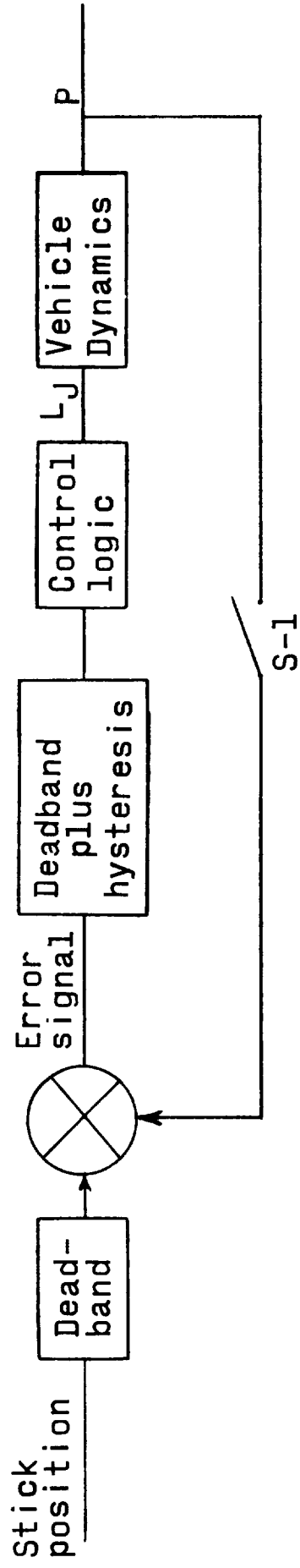
(a) General location.

Figure 3.- Location of control jets.



(b) Rear view (X_b into paper).

Figure 3.- Concluded.



Simplified block diagram of roll control system. Pitch and yaw channels are similar except that no deadband is used for the stick signal.

S-1 is open for direct system and closed for rate-command.

Figure 4.- Block diagram of manual control system.

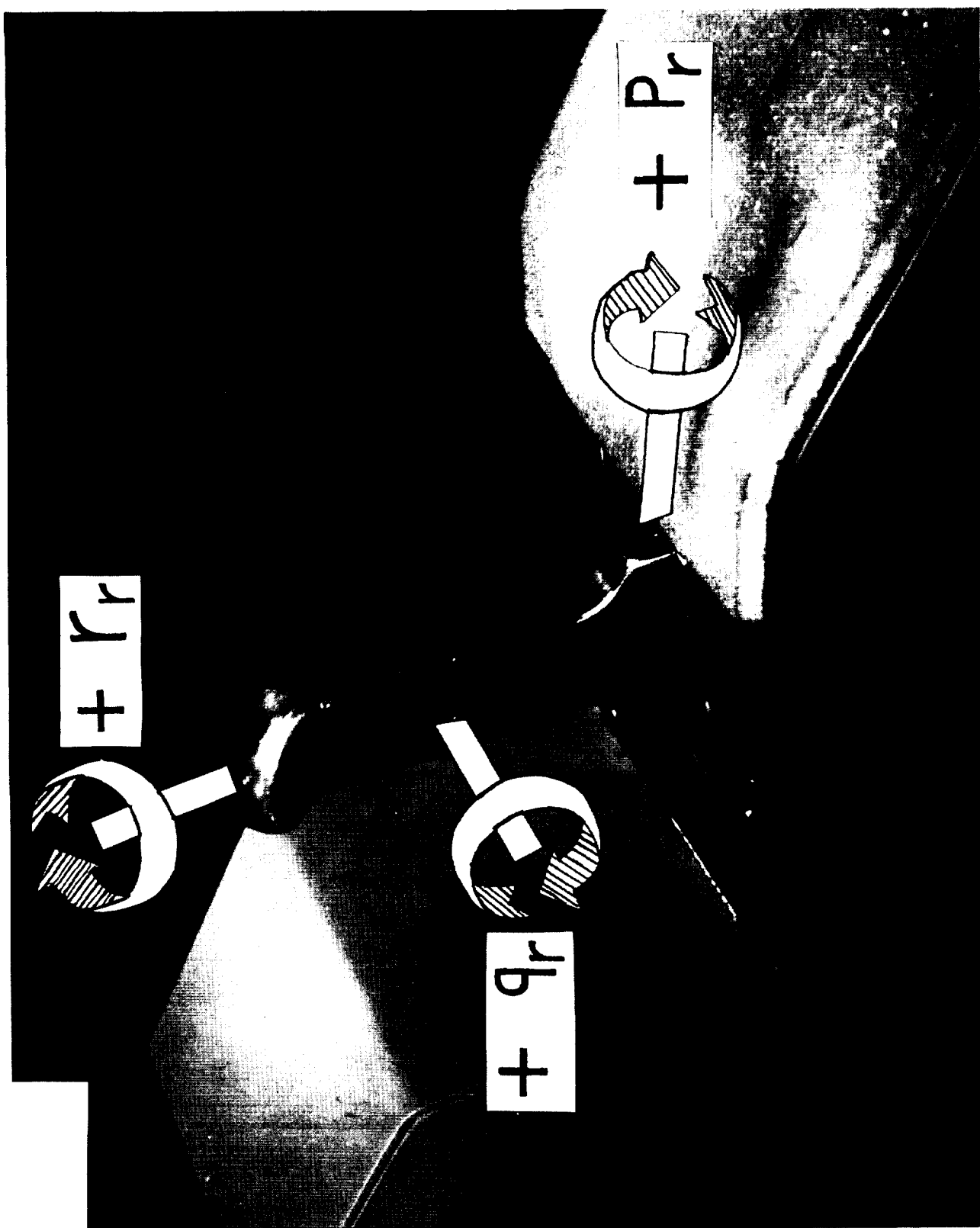


Figure 5.- Hand controller.

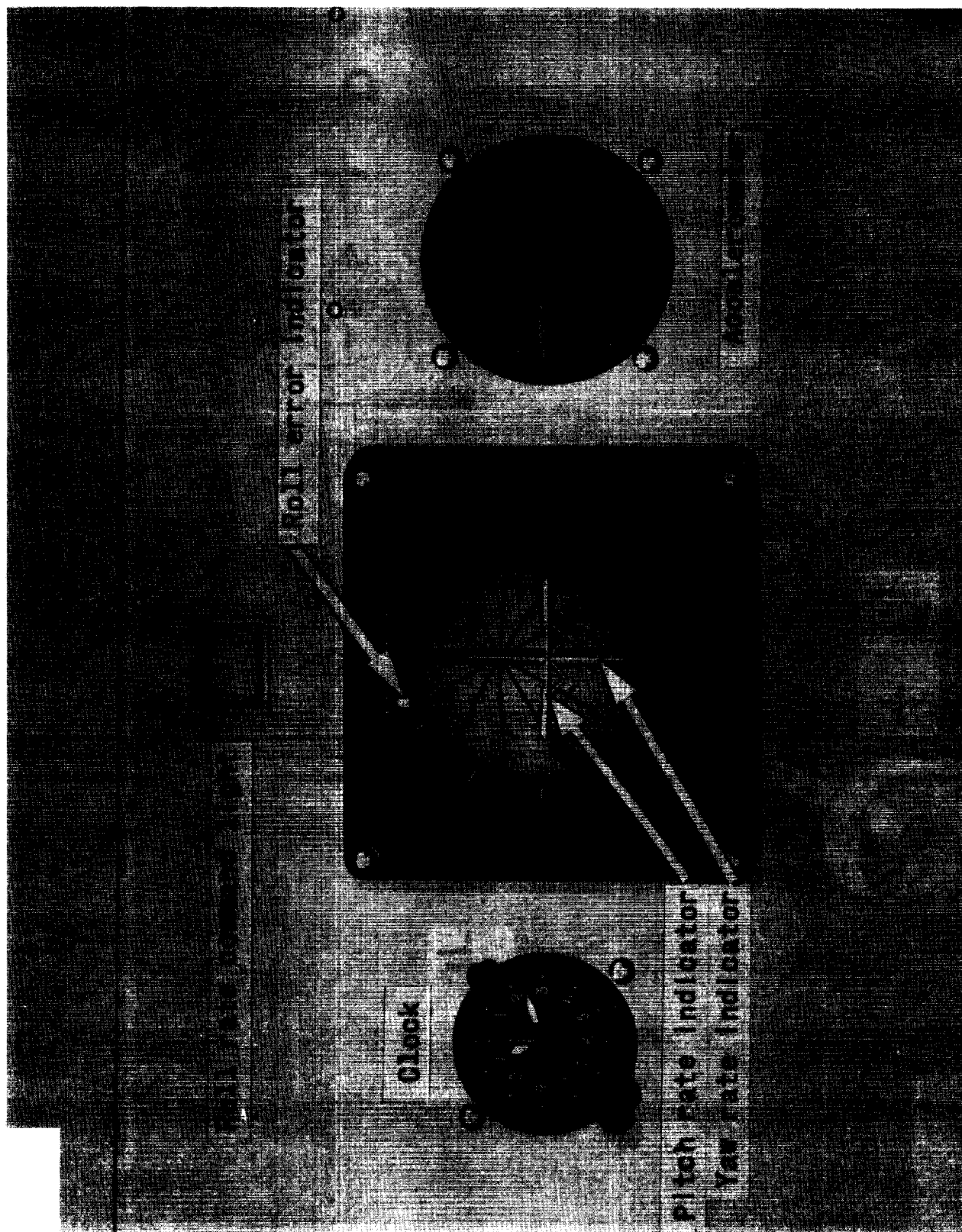


Figure 6.- Display panel.

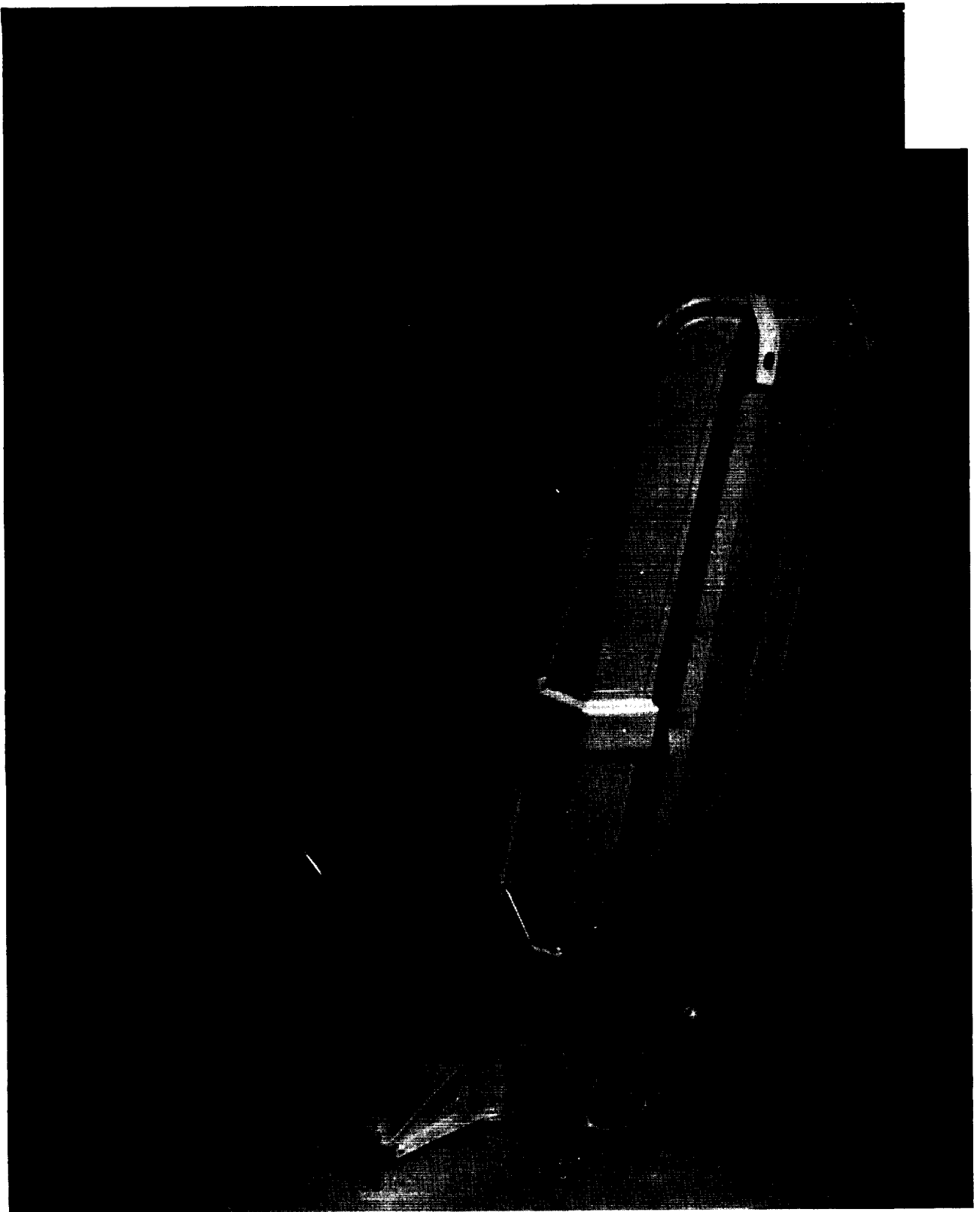
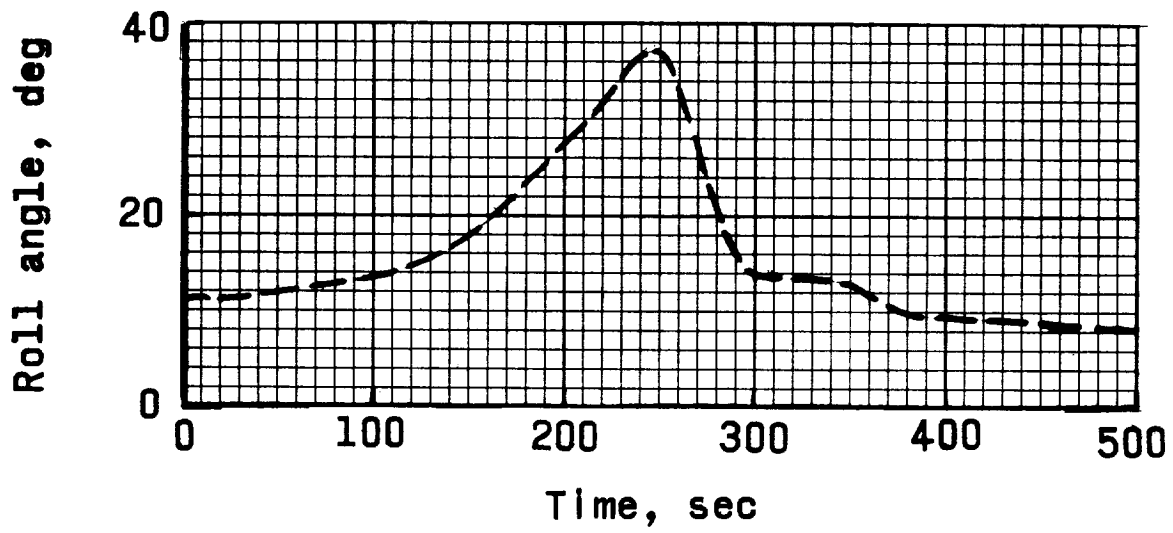
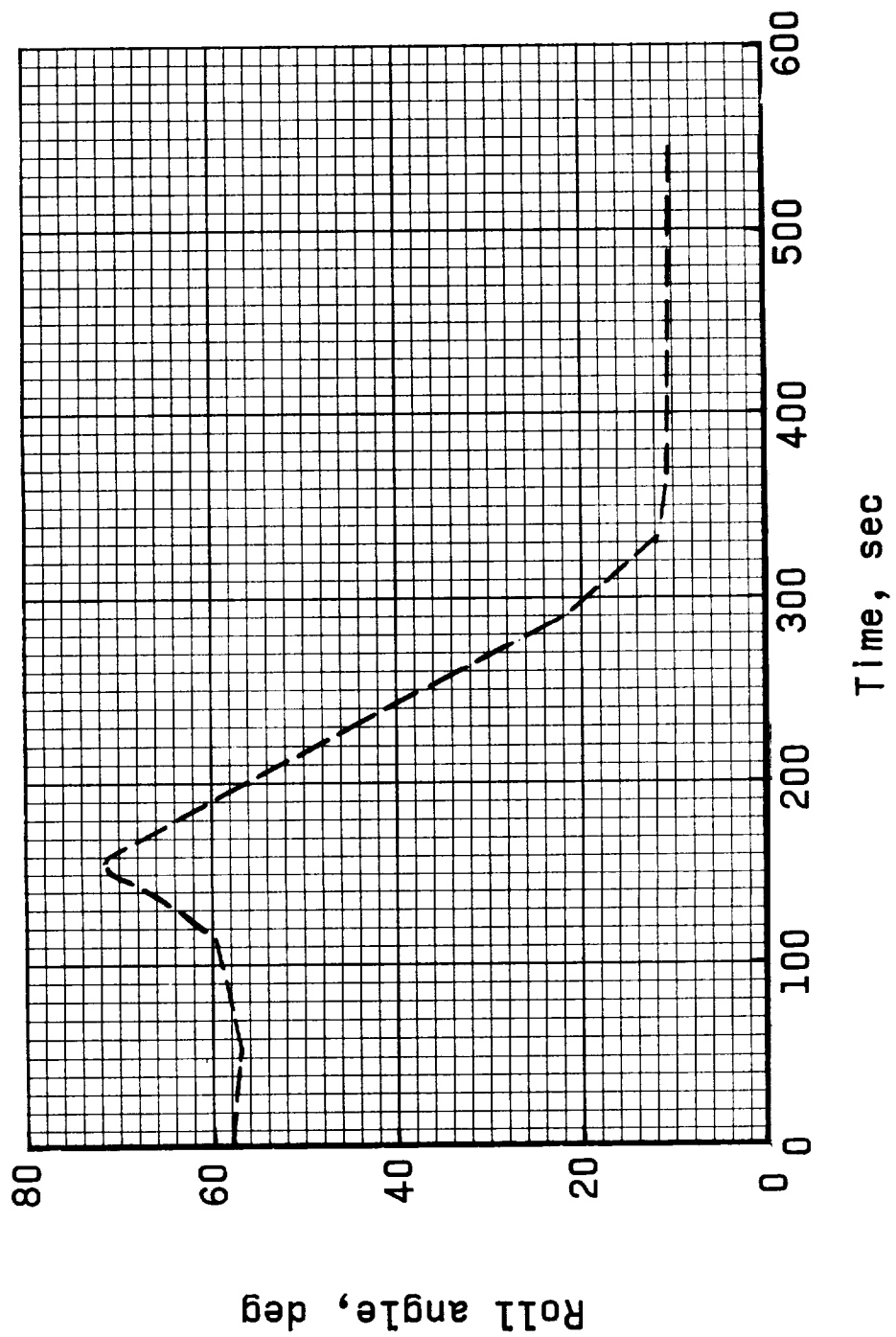


Figure 7.- Simulator cockpit.



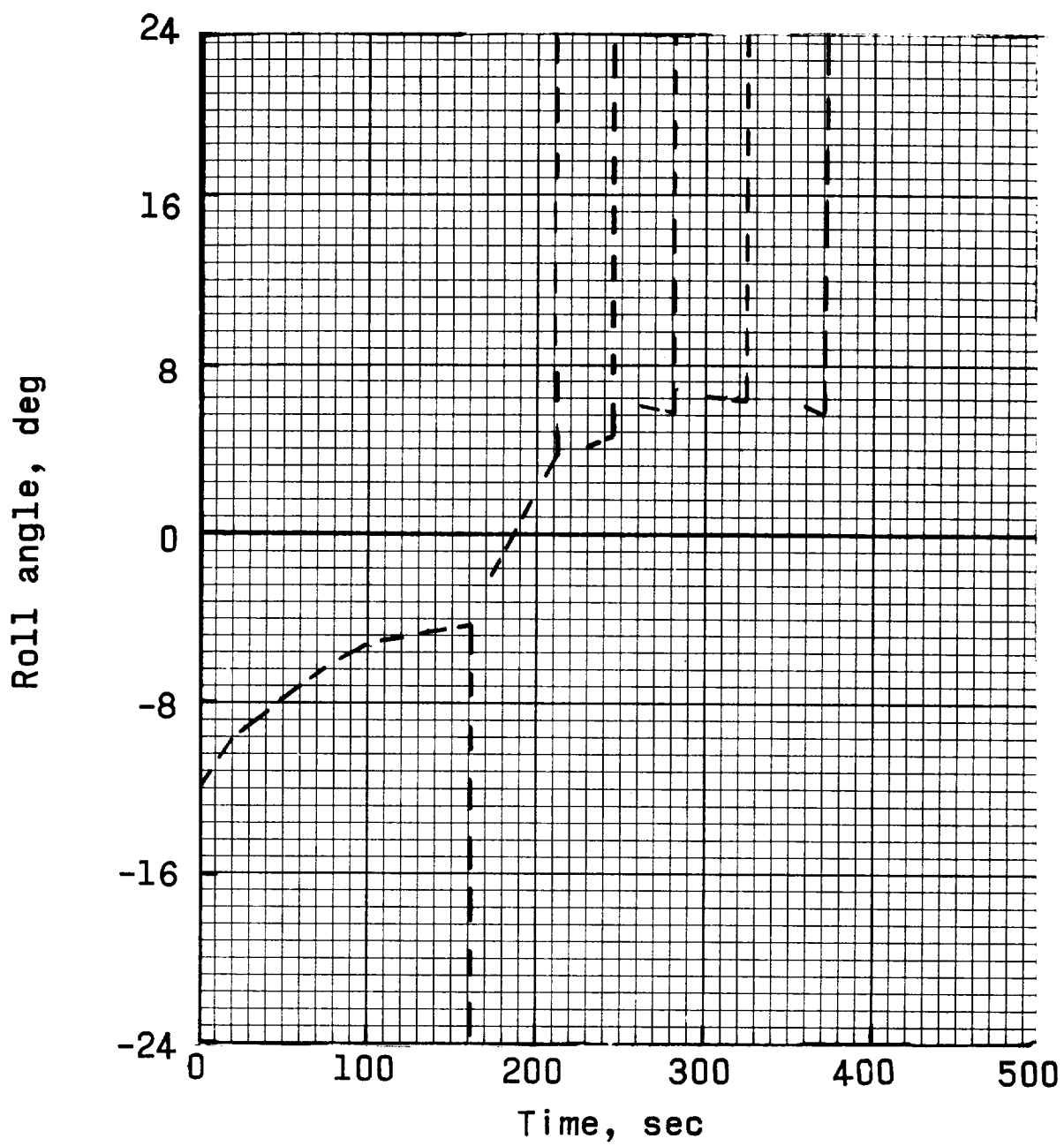
(a) Roll profile A.

Figure 8.- Time histories of commanded roll angles.



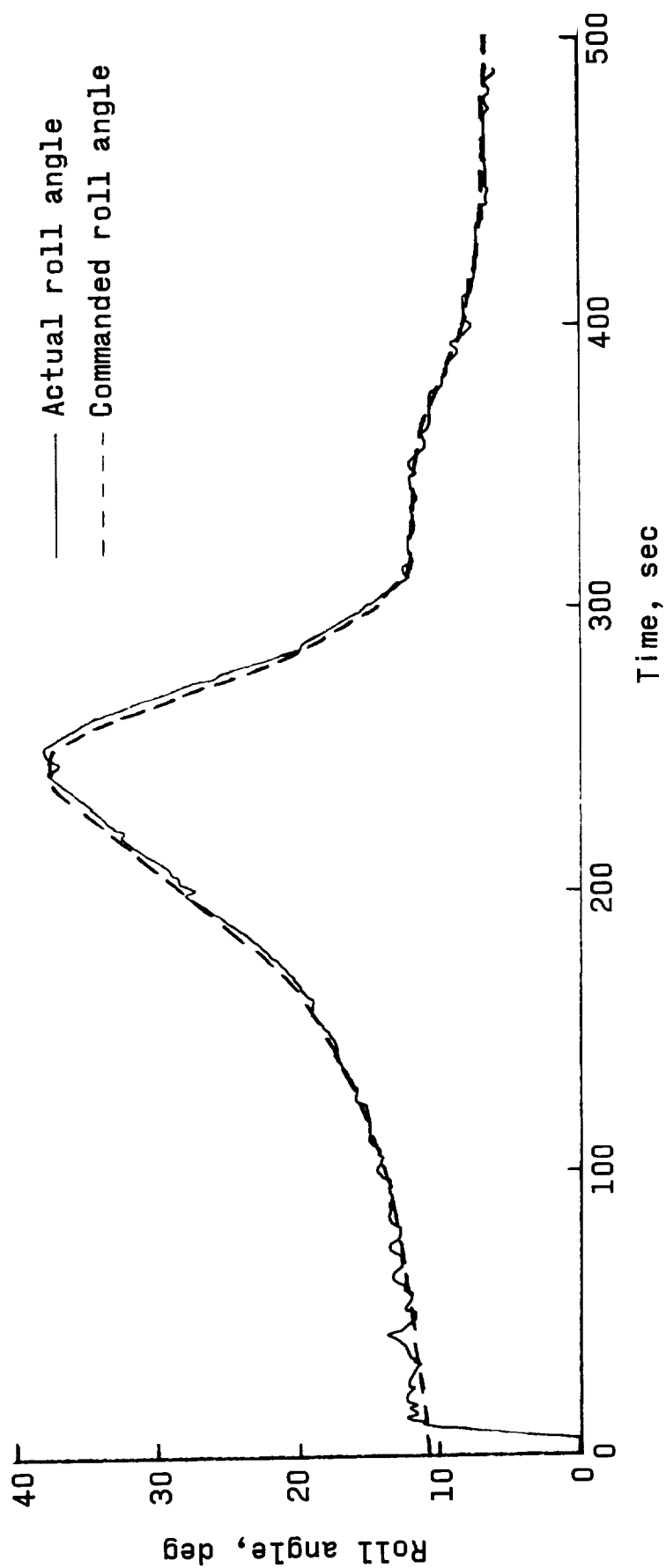
(b) Roll profile B.

Figure 8.- Continued.



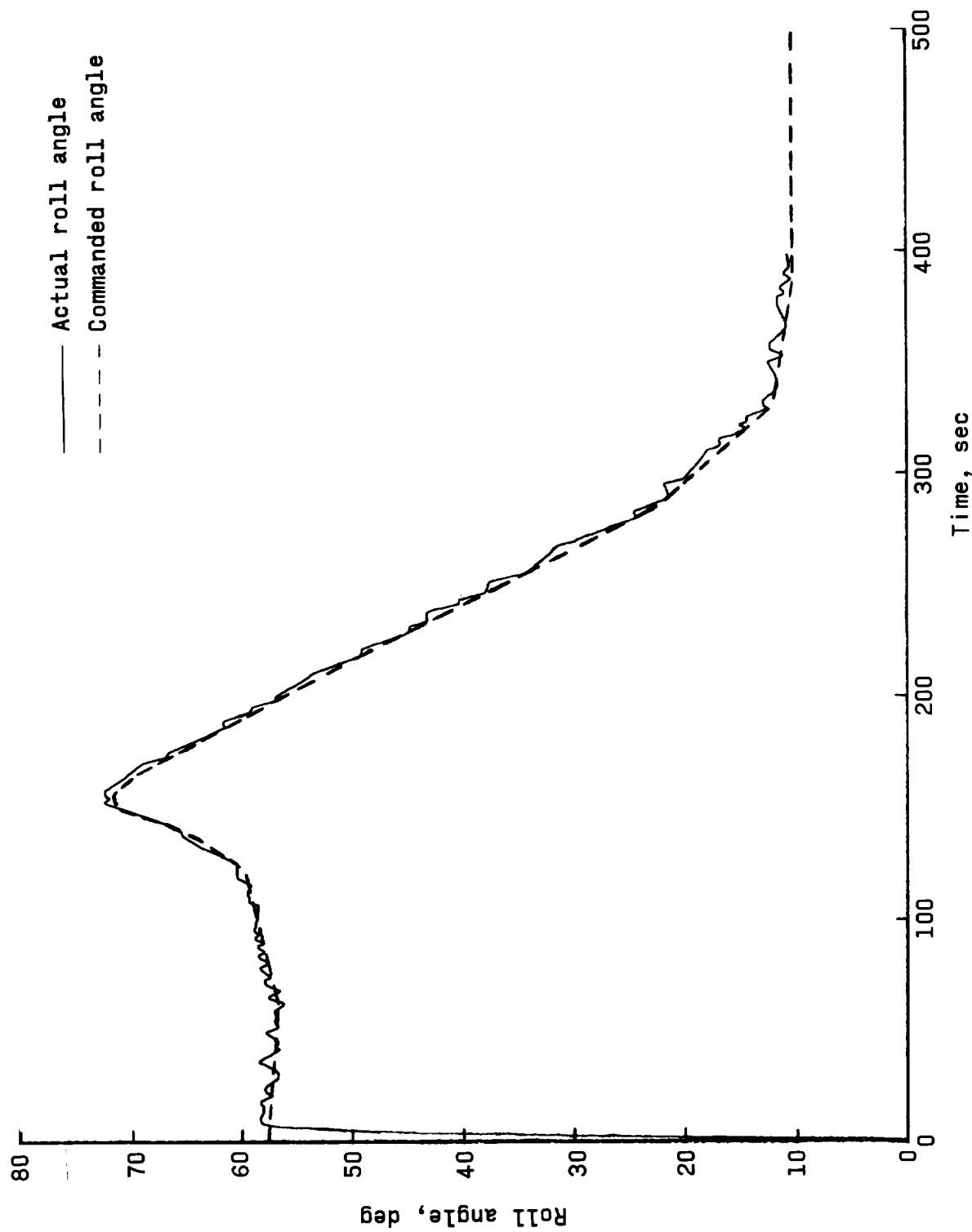
(c) Roll profile C.

Figure 8.- Concluded.



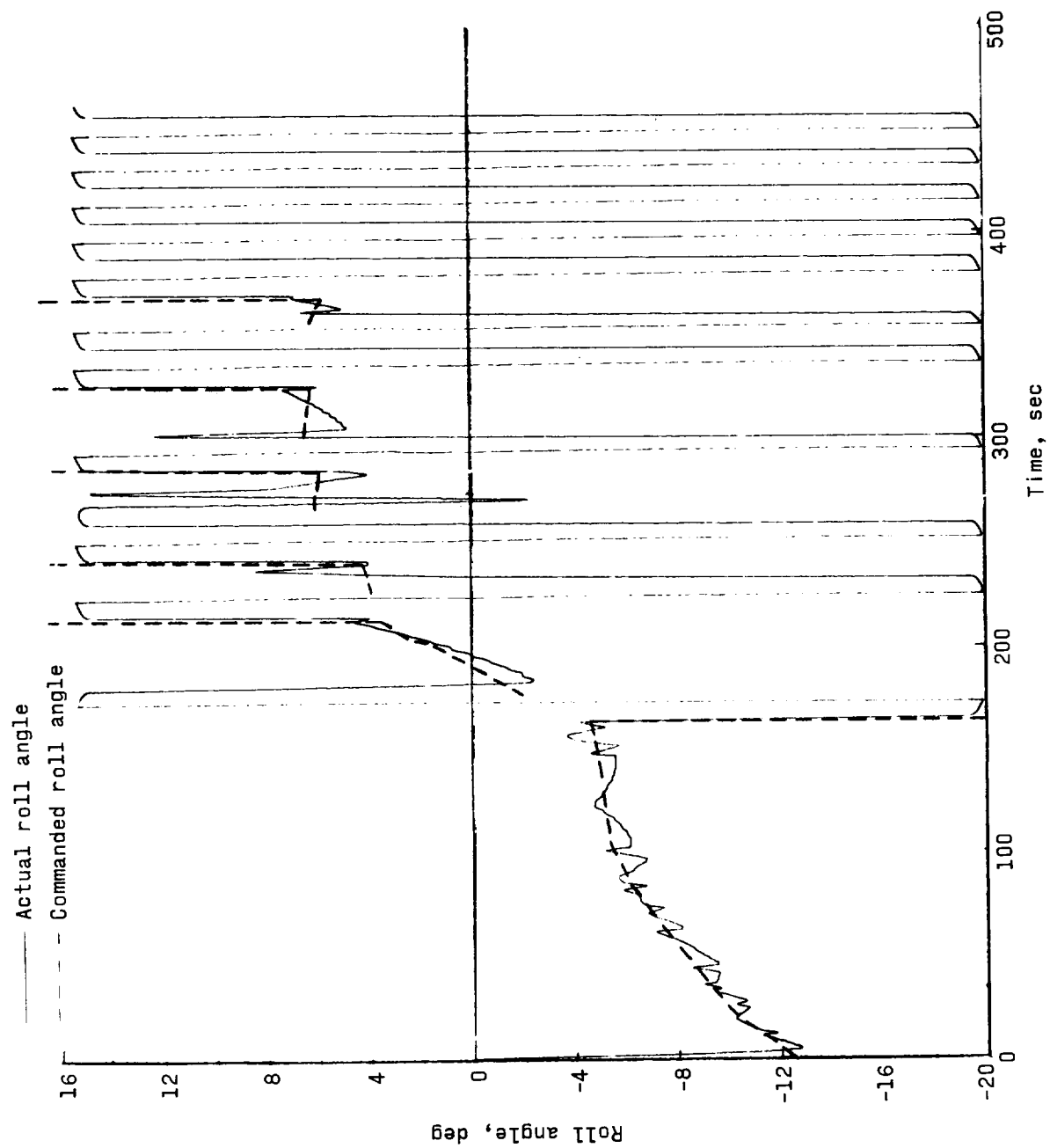
(a) Flight 1, roll profile A, rate-command mode.

Figure 9.- Time histories of actual roll angles and commanded roll angles.



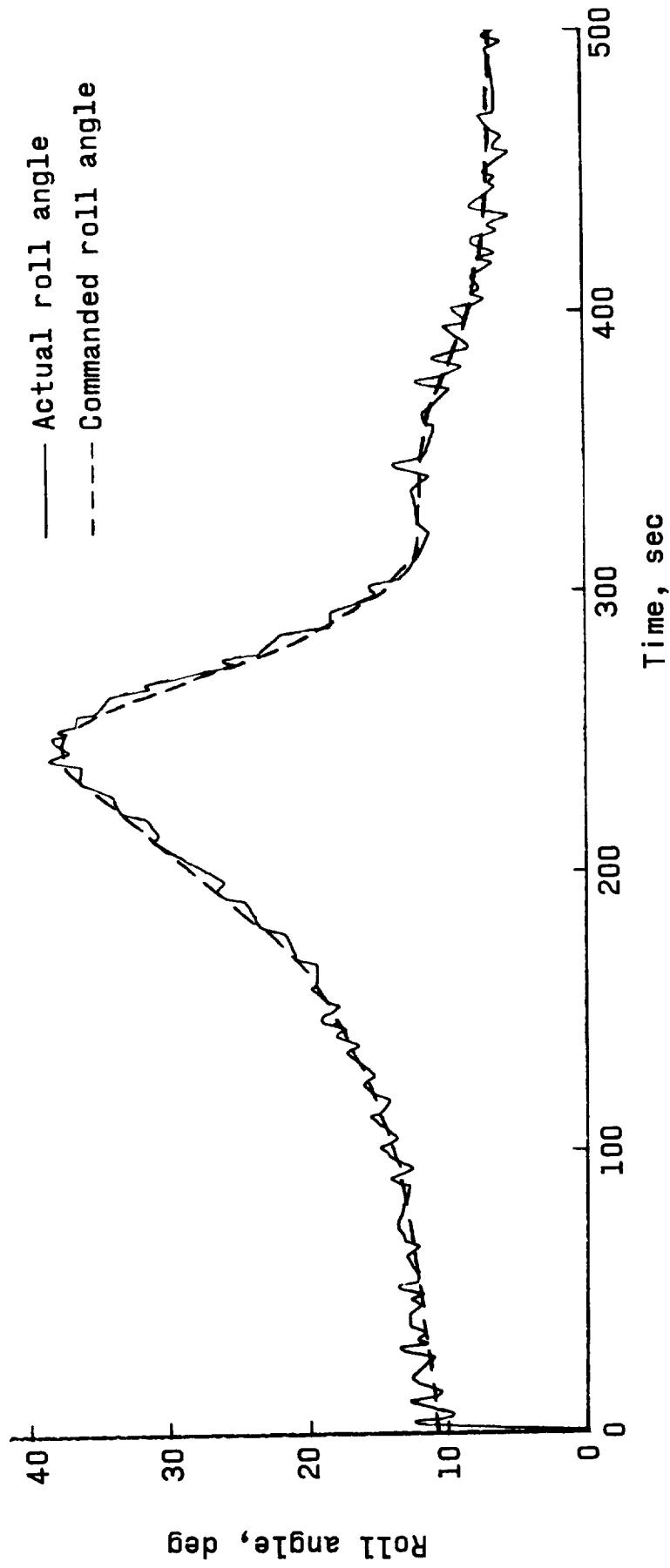
(b) Flight 2, roll profile B, rate-command mode.

Figure 9.- Continued.



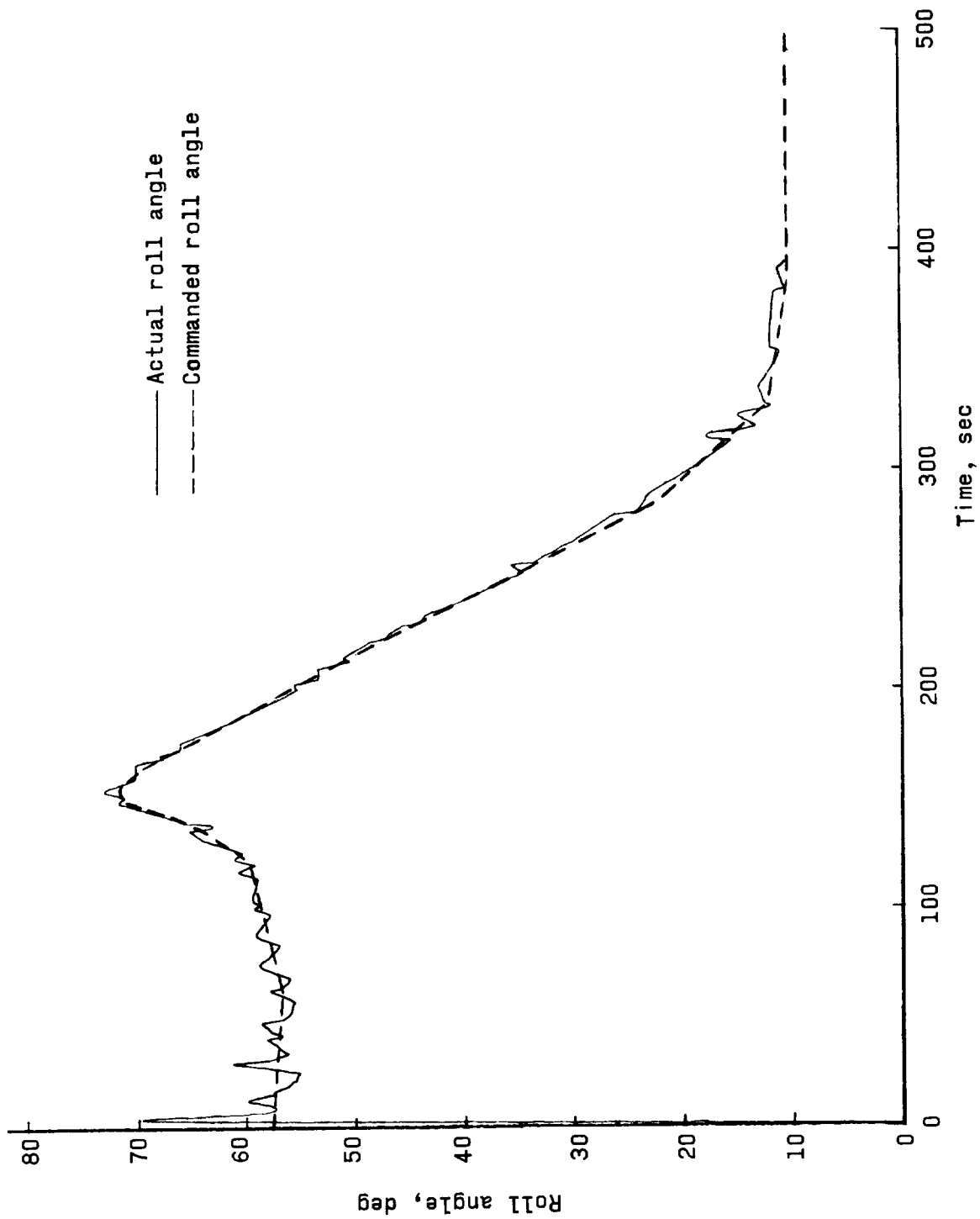
(c) Flight 3, roll profile C, rate-command mode.

Figure 9.- Continued.



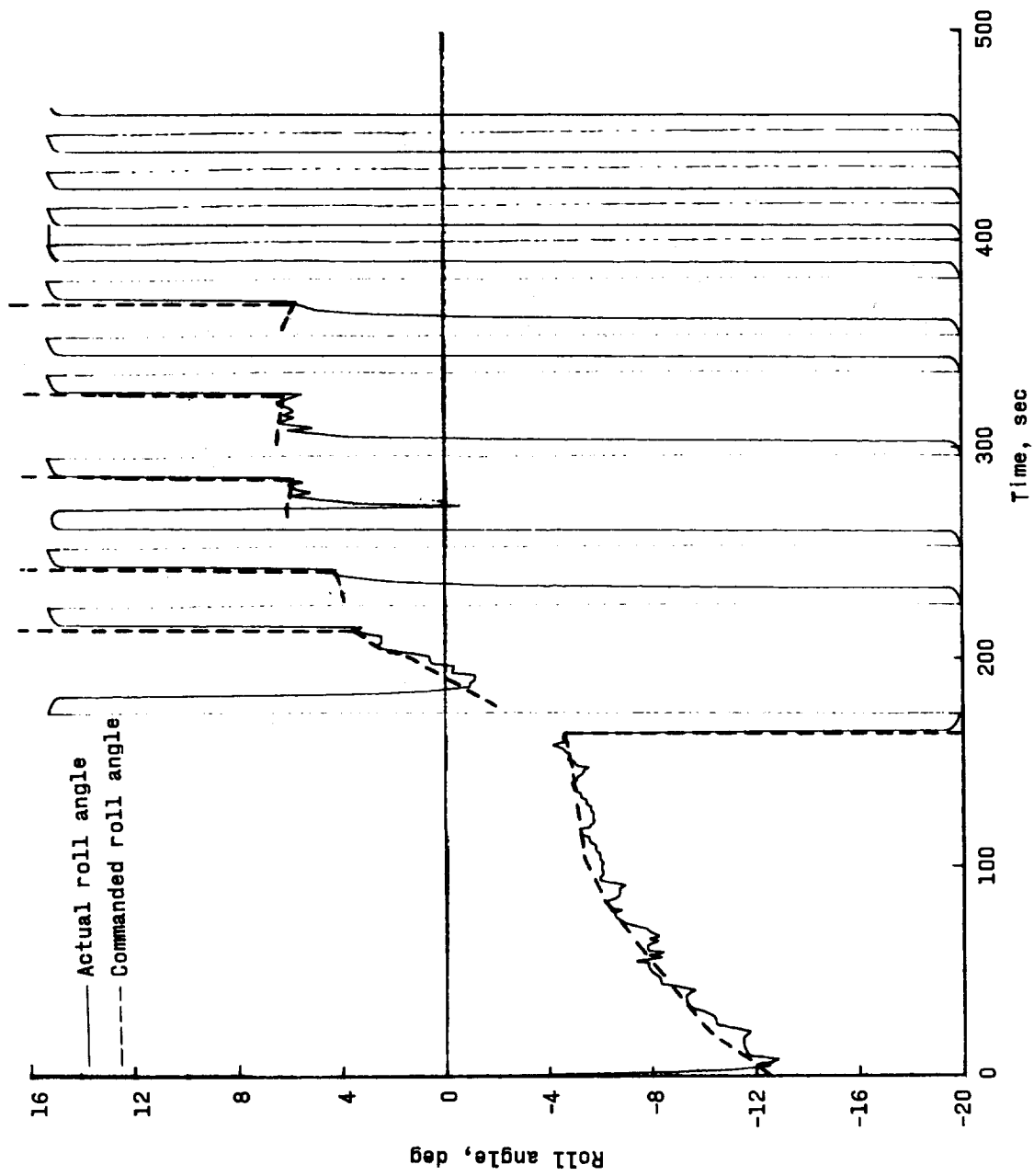
(d) Flight 4, roll profile A, direct mode.

Figure 9.- Continued.



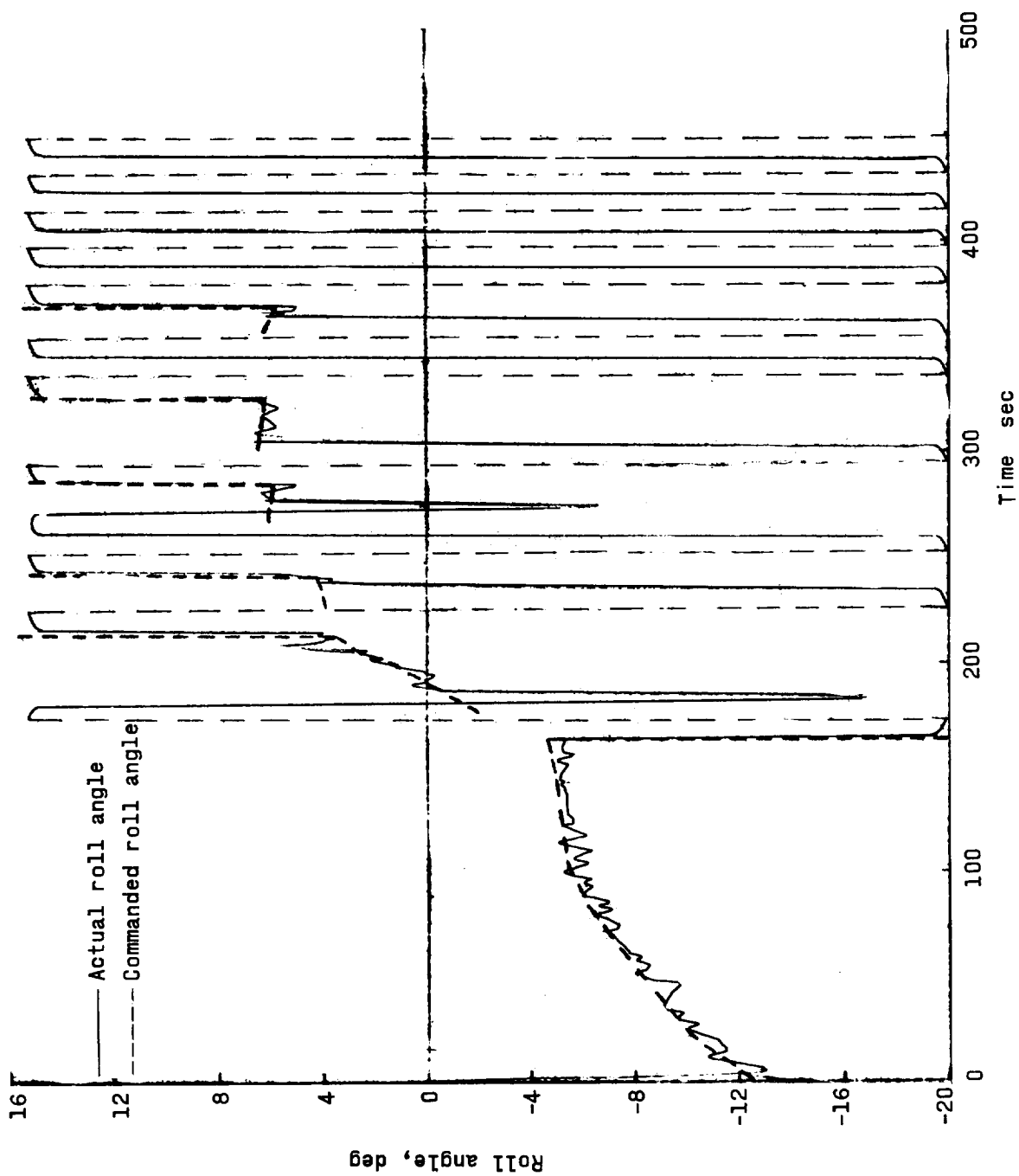
(e) Flight 5, roll profile B, direct mode.

Figure 9.- Continued.



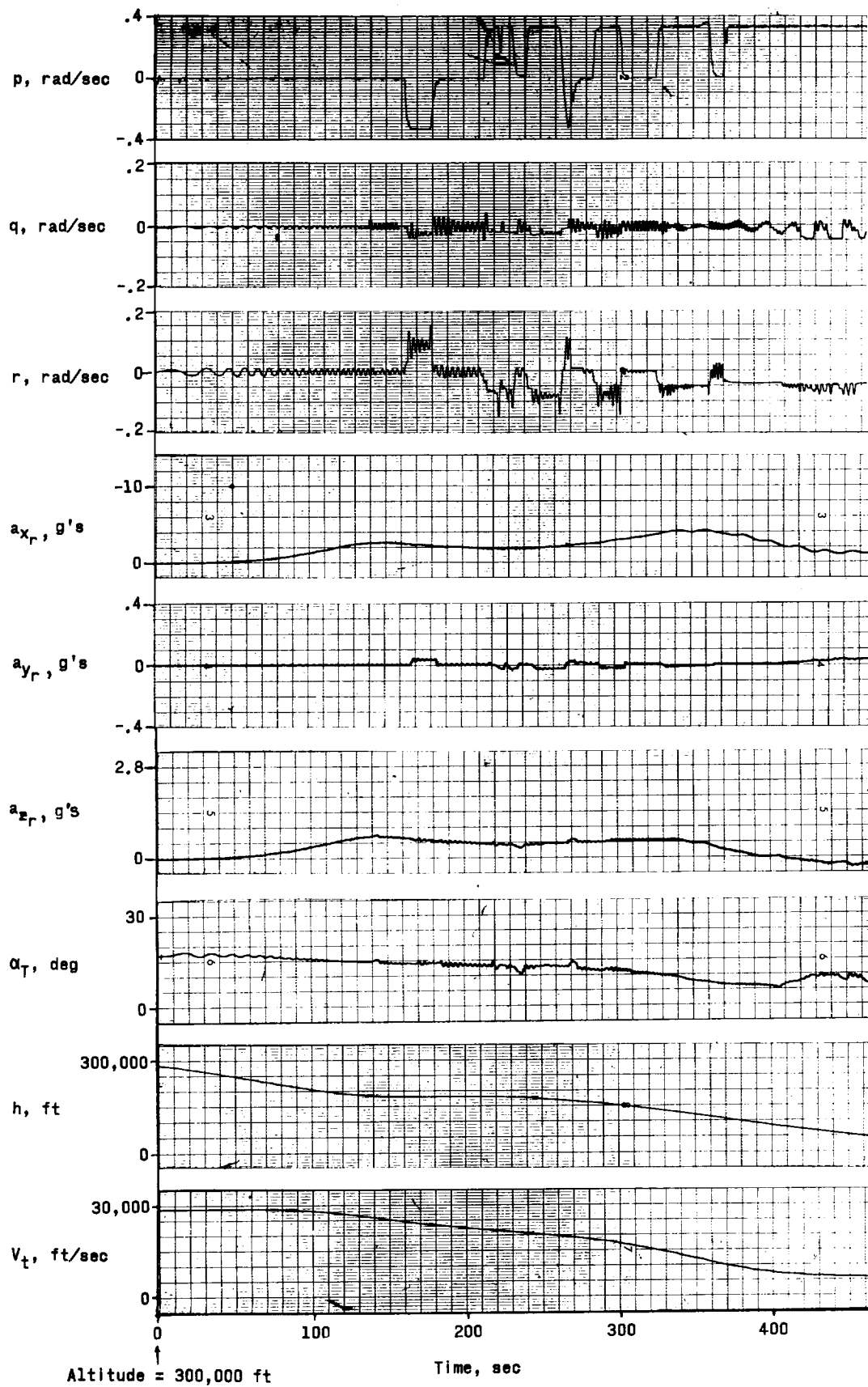
(f) Flight 7, roll profile C, direct mode.

Figure 9.- Continued.



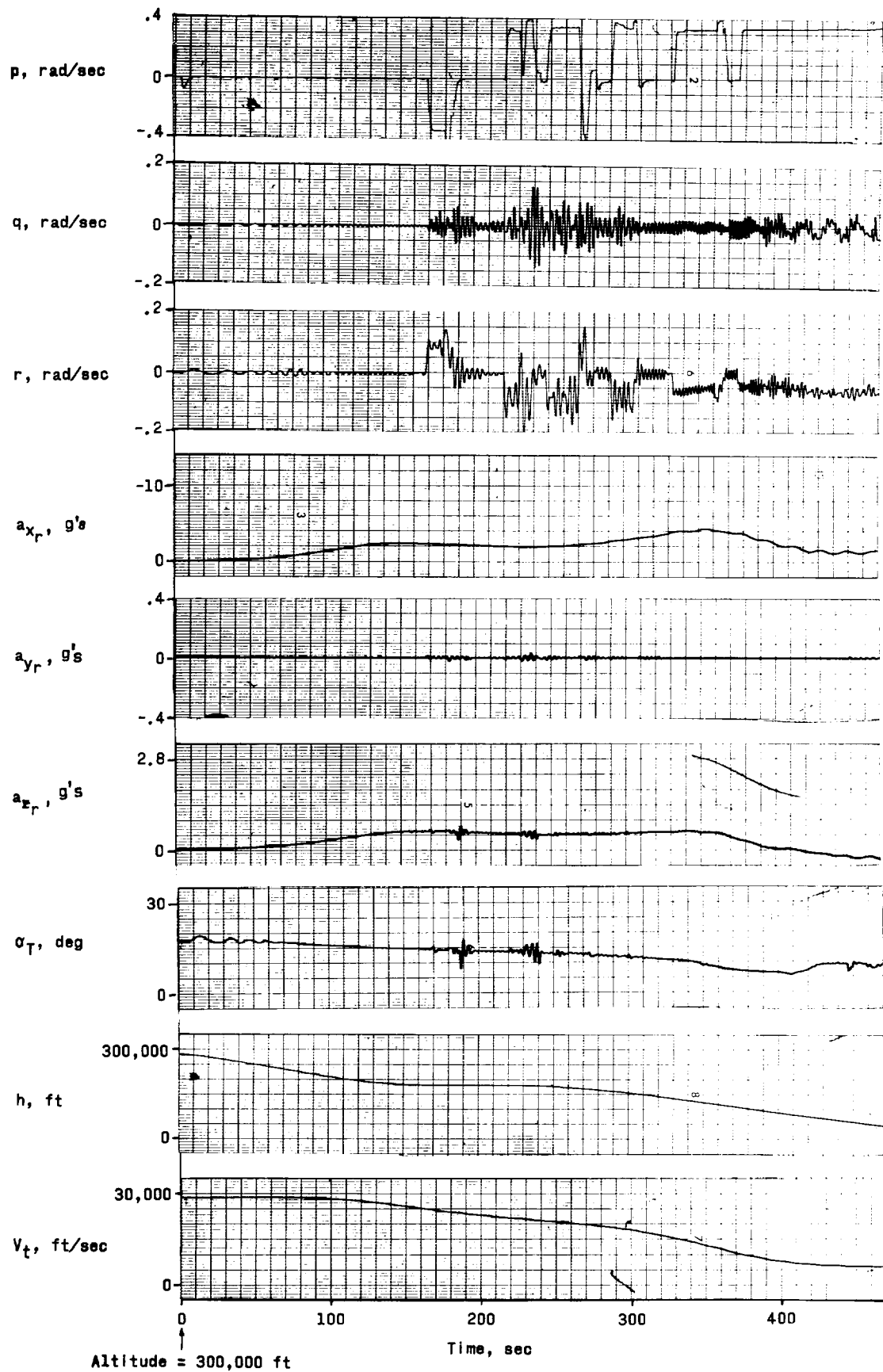
(g) Flight 8, roll profile C, direct mode
One ring of control jets.

Figure 9.- Concluded.



(a) Flight 3, rate-command mode.

Figure 10.- Time histories of atmospheric entries.



(b) Flight 7, direct mode.

Figure 10.- Concluded.

PILOT RATING

47

Pilot _____ Date _____ Flight _____
Mode I, II { I Direct Roll Profile A,B,C, Constant
 { II Rate Command

A. Modifications to Original System:

B. Rating Code:

1. Excellent, includes optimum
2. Good, pleasant to operate
3. Satisfactory, but with some mildly unpleasant characteristics
4. Acceptable, but with unpleasant characteristics
5. Unsatisfactory for normal operation
6. Acceptable for emergency condition only
7. Unacceptable even for emergency condition
8. Unacceptable - dangerous
9. Unacceptable - uncontrollable - unreadable
10. Motions violent - unstable

C. Rating:

1. Eight ball - - - - - _____
2. Pitch and yaw indicators - - - - - _____
3. Roll error indicator - - - - - _____
4. Hand controller - - - - - _____
5. Control jet moments and vehicle response - - - - - _____
6. Integrated system - - - - - _____

D. Comments:

Figure 11.- Pilot rating sheet.

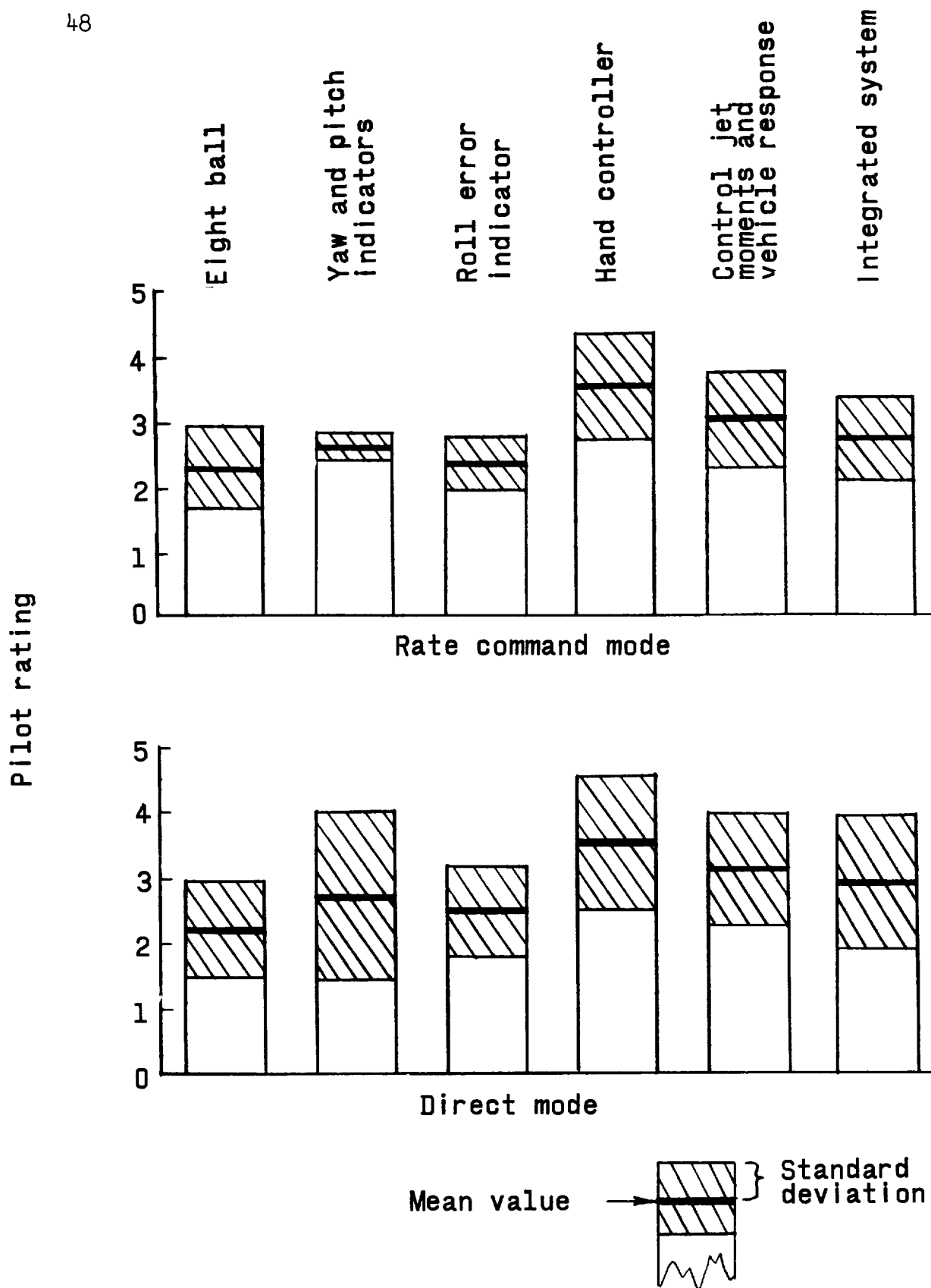
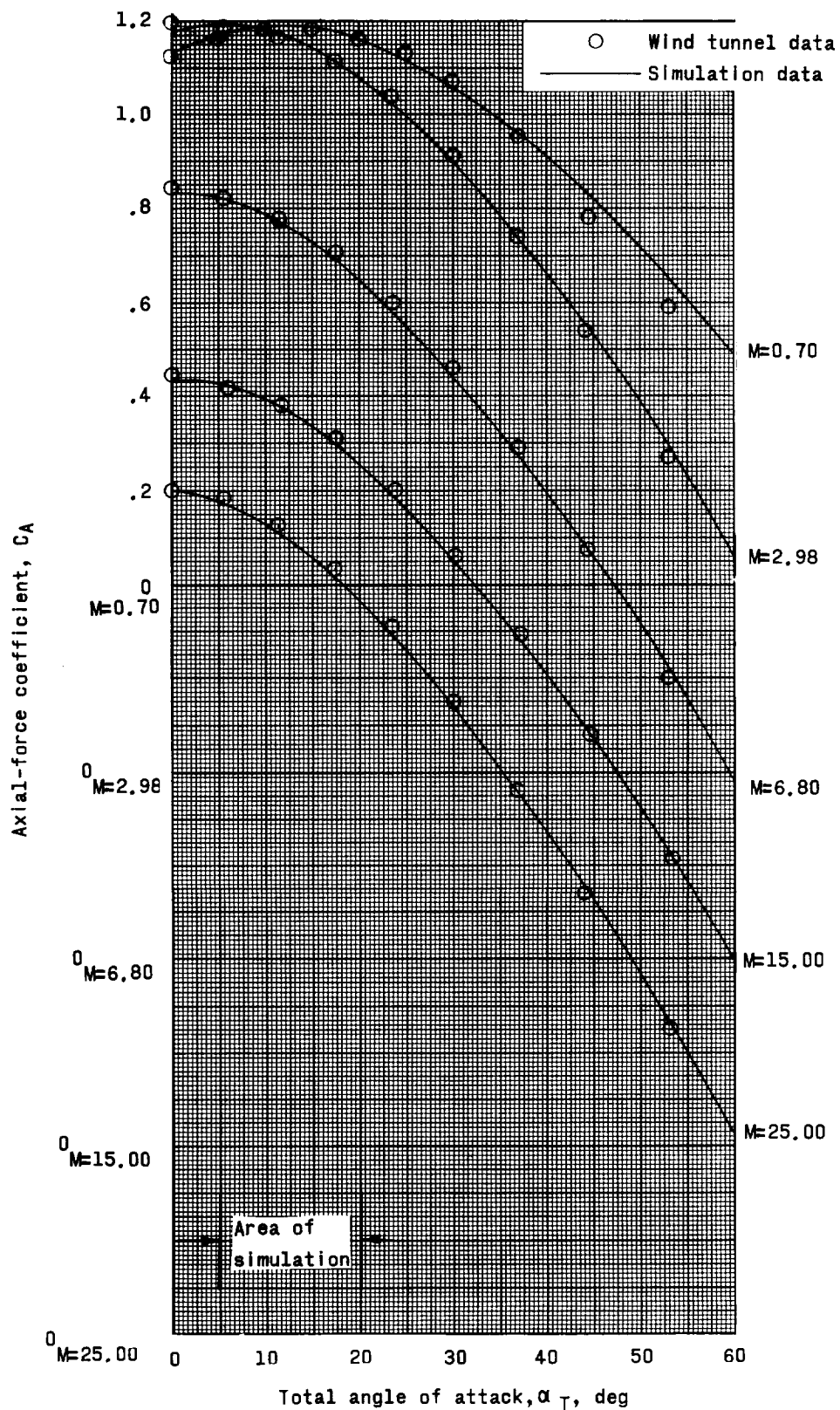
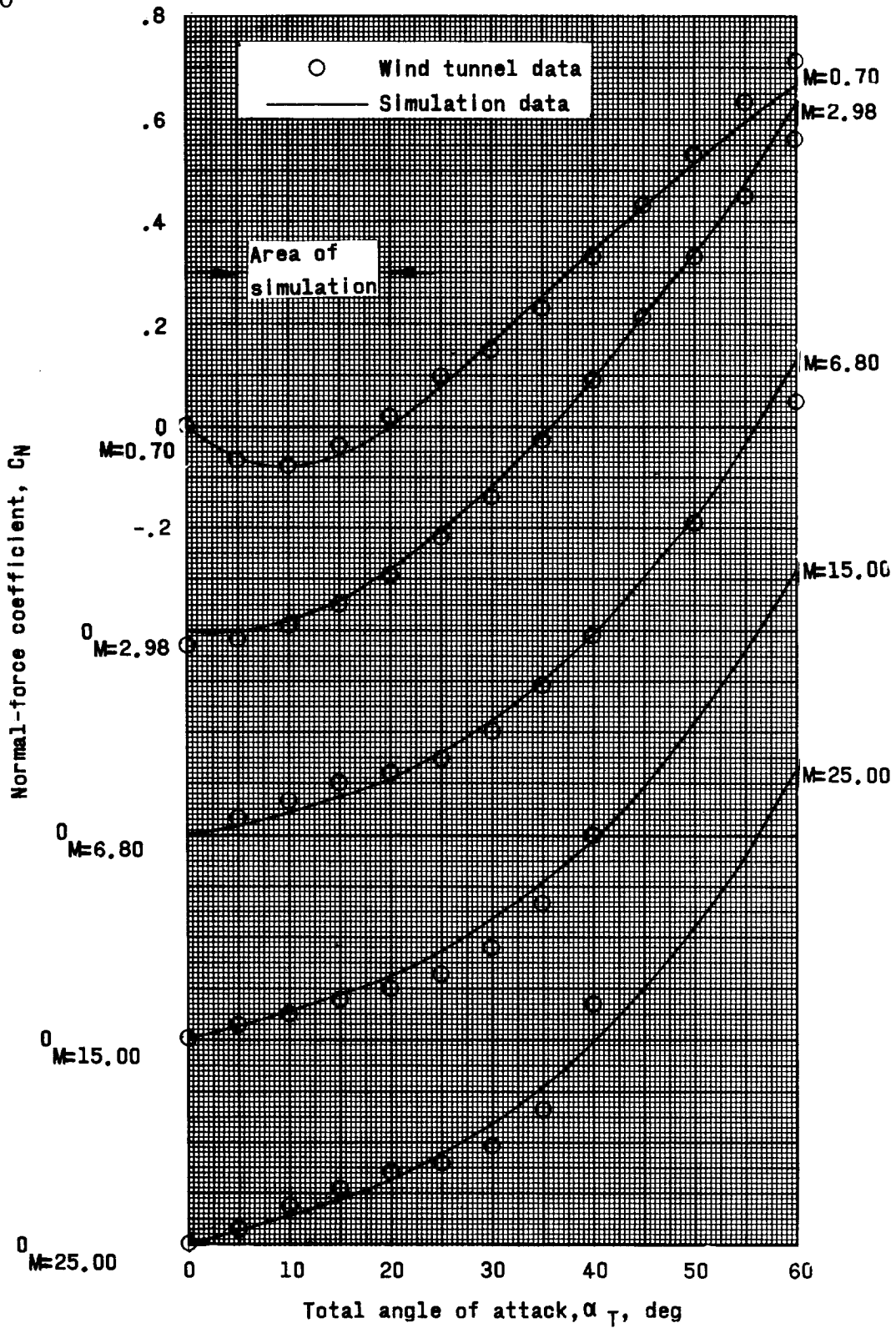


Figure 12.- Pilot rating summary.



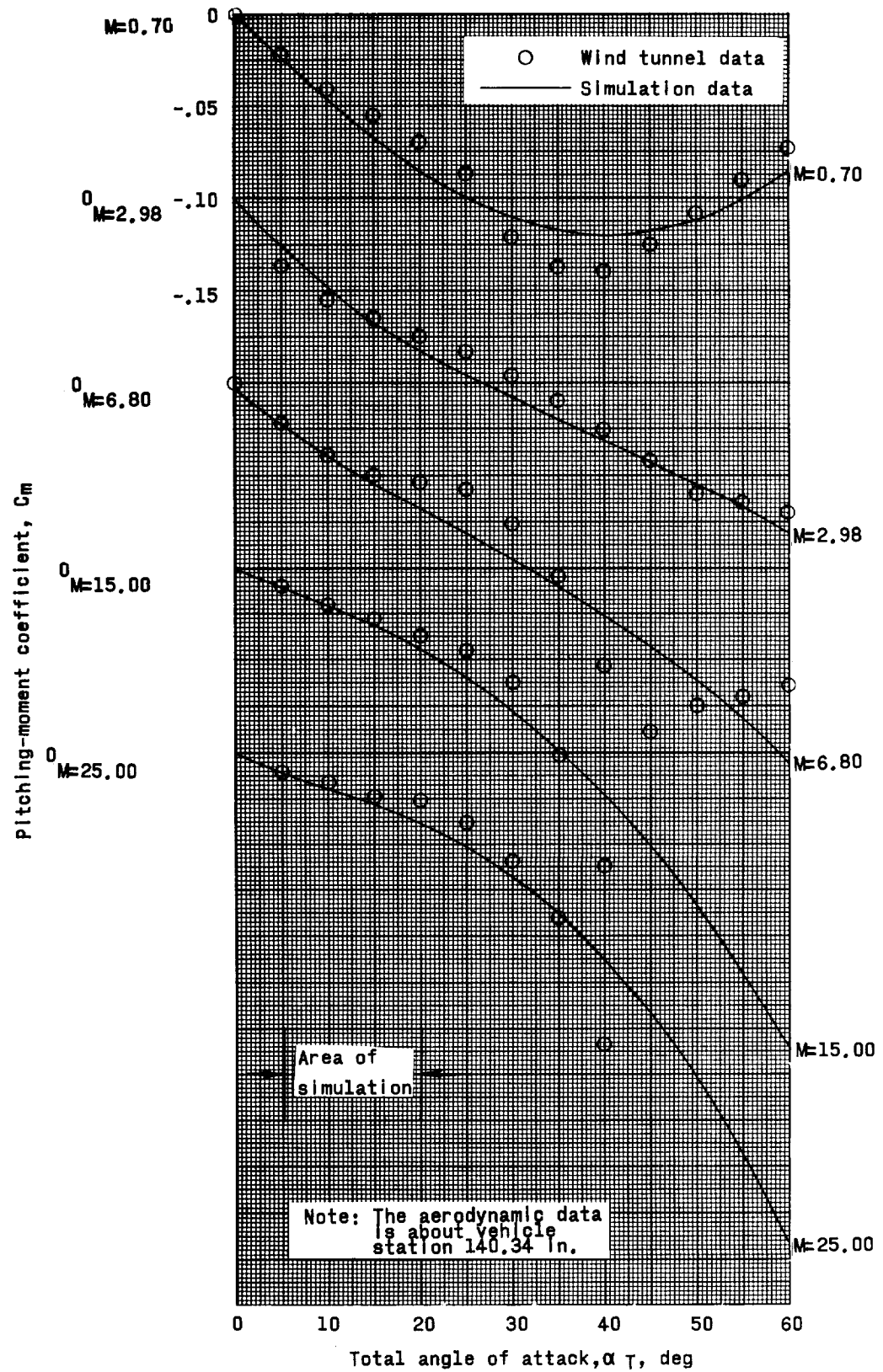
(a) Axial-force coefficient.

Figure 13.- Aerodynamic characteristics of simulated vehicle.



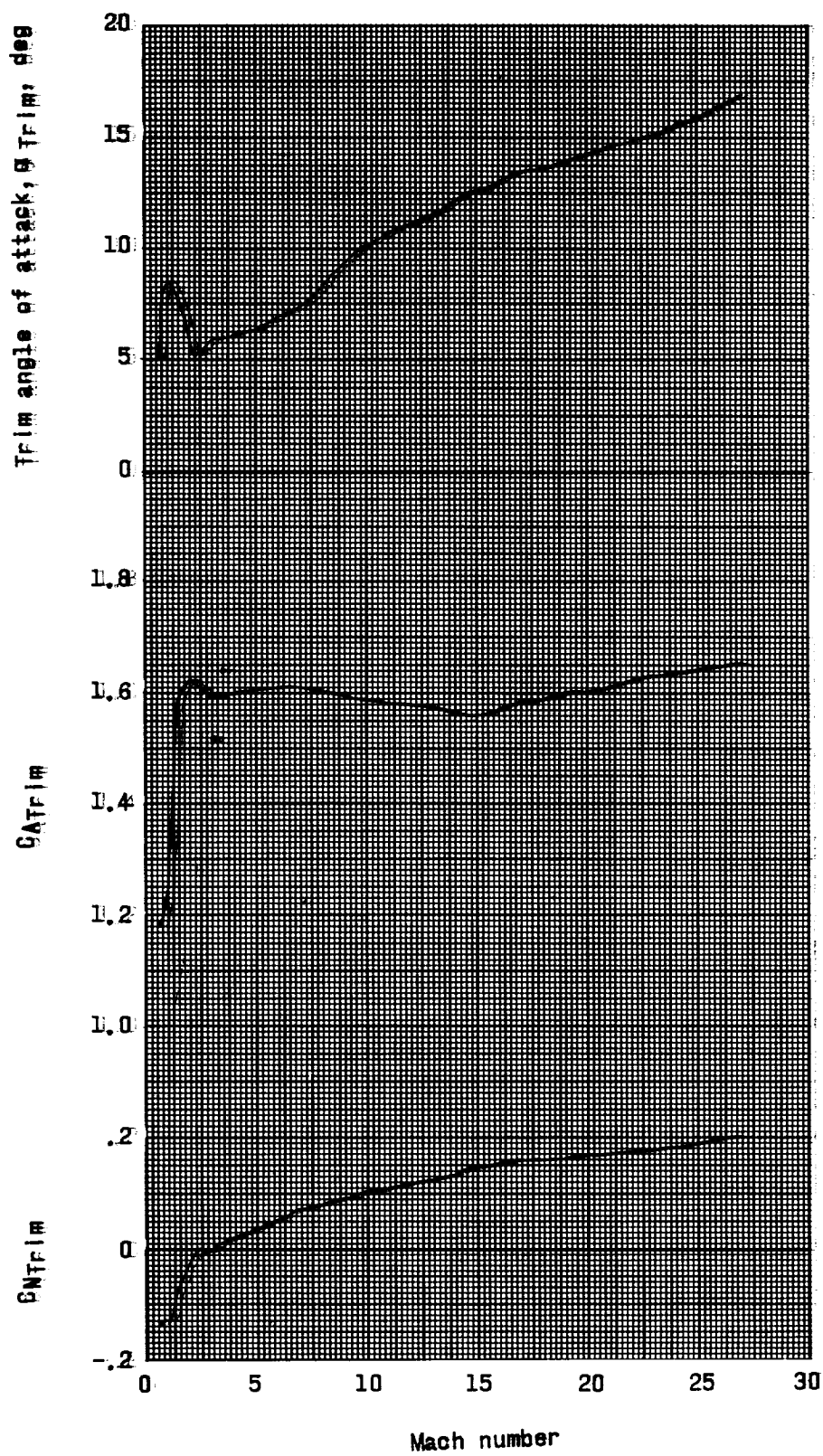
(b) Normal-force coefficient.

Figure 13.- Continued.



(c) Pitching-moment coefficient.

Figure 13.- Continued.



(d) Trim conditions.

Figure 13.- Concluded.